protein. Female mice of the genotypes of wild-type ($ARH^{+/+}$), $ARH^{+/-}$, $ARH^{-/-}$, and $LDLR^{-/-}$, 12 to 15 weeks of age, were fasted for 13 hours. Three mice in each genotype received an intravenous bolus via the external jugular vein of ^{125}I-labeled mouse LDL (5 μg of protein). Blood was collected from the tail vein with heparinized Pasteur pipette at the indicated timings. The plasma ^{125}I-labeled apoB was measured by isopropanol precipitation, followed by gamma counting as previously described.[17]

In Vivo Hepatic Uptake of Intravenously Injected DiI-LDL

Twelve-week-old female mice of the genotypes of wild-type, $ARH^{-/-}$, and $LDLR^{-/-}$ were fasted for 13 hours. Each mouse received an intravenous bolus via the external jugular vein of 50 μg of human DiI-LDL (Molecular Probes Inc, Eugene, Ore). To detect nonspecific incorporation of DiI-LDL, 2.5 mg of unlabeled human LDL was injected 2 minutes before 50 μg of DiI-LDL was injected. Two minutes after DiI-LDL injection, blood was collected for determination of cholesterol and lipoproteins. After 4 hours, the right atrium was punctured, 10 mL of phosphate-buffered saline (PBS) was injected via the left ventricle, and subsequently 10 mL of PBS containing 4% paraformaldehyde. The tissues were immersed in PBS containing 4% paraformaldehyde at 4°C for 12 hours. The liver samples were frozen in liquid nitrogen and subjected to microscopic analysis. To stain Kupffer cells, BM8 (rat antibody against mouse pan-macrophage) (BMA Biomedicals AG, Augst, Switzerland) was used as a primary antibody and fluorescein isothiocyanate-conjugated rabbit anti-rat IgG (DAKO Cytomation, Glostrup, Denmark) was used as a secondary antibody. The samples were observed by confocal laser scanning microscopy (LSM5 PASCAL; Zeiss, Co, Tokyo, Japan).

Labeling of Human LDL With ^{3}H-CE

LDL was labeled with ^{3}H-CE according to the previously described method,[21] with a minor modifications.

In Vivo Hepatic Uptake of Intravenously Injected ^{3}H-CE-LDL

^{3}H-CE-LDL (0.8 μCi) was injected via the external jugular vein of wild-type ($ARH^{+/+}$), $ARH^{-/-}$, and $LDLR^{-/-}$ female mice, 12 to 15 weeks of age. Blood was collected from the tail vein with heparinized Pasteur pipette at 2 minutes and 4 hours after the injection. The blood was dispersed in chloroform/methanol, 2/1 (v/v). Immediately after the second blood collection, 2 mg of human LDL was injected via the inferior vena cava. Ten minutes later, the right atrium was punctured and 20 mL of PBS was injected via the left ventricle three times to wash the blood from the body. The liver was isolated, immersed in chloroform/methanol 2/1 (v/v), and homogenized with a polytron homogenizer. The lipid was extracted from the liver and the blood by the method of Folch.[22] Radioactivity in each sample was counted in a liquid scintillation counter using a scintillation cocktail of toluene/Triton X100 (2:1) containing PPO (0.6%) and POPOP (0.05%).

Preparation and Culture of Mouse Hepatocytes

Mice (14 to 16 weeks of age) of the indicated genotype were used for the study. The livers were perfused via the portal vein and hepatocytes were obtained by the method of Seglen.[23] After 24-hour incubation in Waymouth MB 752/1 medium containing 10% fetal calf serum in six-well plates, the cells were subjected to the study.

In Vitro Uptake of ^{3}H-CE-LDL Into Primary Cultured Hepatocytes

The cells were incubated in Waymouth MB 752/1 medium containing 10% LPDS for 48 hours, and then incubated in DMEM containing 2% bovine serum albumin (without free fatty acid) and ^{3}H-CE-LDL (5 to 100 μg/mL) for an additional 3 hours. Then, the cells were washed twice with 150 mmol/L NaCl, 50 mmol/L of Tris-HCl (pH 7.4) containing 2 mg/mL of bovine serum albumin, and once with the same buffer without bovine serum albumin. The cells were incubated with LDL-releasing buffer (50 mmol/L NaCl, 10 mmol/L Hepes (pH 7.4), containing 10 mg/mL heparin) at 4°C for 1 hour. After removal of the heparin-releasable fraction, 1 mL of hexane/isopropyl alcohol (3/2) was added to the cells to extract lipids in the cells.[24] After delipidation, the cells were dissolved in 1 N NaOH and protein concentration was measured.

^{125}I-LDL Binding, Incorporation, and Degradation Assays

Waymouth MB 752/1 medium containing 10% LPDS was added to the cells and incubated for another 24 hours. Binding, internalization, and degradation of ^{125}I-LDL were analyzed according to the method previously described.[25]

DiI-LDL Incorporation Into Primary Cultured Hepatocytes

The cells were added to Waymouth MB 752/1 medium containing 10% LPDS and incubated for 24 hours. Then, the cells were washed twice and incubated at 37°C for 3 hours with 50 μg/mL of DiI-LDL in 0.2 mL of MEM containing 10% LPDS. Nonspecific incorporation was determined by parallel incubation in the presence of 20-fold excess of LDL. The cells were washed three times with PBS containing 0.2% bovine serum albumin, followed by washing twice with PBS. The samples were observed with a laser confocal microscopy.

An expanded Materials and Methods section is available in the online data supplement at http://circres.ahajournals.org.

Results

Generation of *ARH* Knockout Mice

OmniBank Sequence Tag 149604 (Lexicon Genetics Inc) corresponded to the insertion mutation in the third intron of *ARH* gene in mouse chromosome 4 (Figure 1A). The mutated allele encodes a marker fusion transcript and OmniBank Sequence Tag fusion transcript instead of *ARH* mRNA. The offspring heterozygous animals were mated to produce $ARH^{+/+}$, $ARH^{+/-}$, and $ARH^{-/-}$ mice. Southern blot analysis was performed to genotype the mice using a probe comprising portions of mouse *ARH* gene containing both exon 3 and intron 3 (Figure 1B) after digestion of DNA with *Apa*I. *Apa*I site is not present in the insertion fragment used for development of the knockout mice. Southern blot analysis with the exon probe showed a 3405-bp band for the wild-type allele and was observed in both the wild-type and $ARH^{+/-}$ mice, whereas an 8581-bp band, the disrupted allele which was produced by the insertion of 5176-bp fragment (Figure 1A), was observed in $ARH^{+/-}$ and $ARH^{-/-}$ mice after digestion of DNA with *Apa*I. Southern blot analysis with neo gene probe demonstrated that only one position and one copy insertion event occurred in a mouse genome because $ARH^{+/-}$ and $ARH^{-/-}$ exhibited an 8581 bp.

To confirm that the mutated allele does not express the mRNA, total RNA was isolated from the livers of the animals of each genotype and analyzed by reverse-transcription polymerase chain reaction (Figure 1C). A 944-bp band, the *ARH* transcript that was expressed in wild-type and $ARH^{+/-}$mice, was not detectable in $ARH^{-/-}$ mice. The results thus confirmed that the insertion mutation by gene trap vector disrupted the *ARH* gene expression.

TABLE 1. Lipid and Lipoprotein Profiles of ARH Knockout Mice (mean±SEM)

	Total Cholesterol, mmol/L	Triglyceride, mmol/L	HDL Cholesterol, mmol/L	LDL Cholesterol, mmol/L
Wild type				
Male (n=5)	2.68±0.14	1.04±0.26	2.49±0.12	0.17±0.05
Female (n=8)	2.57±0.22	0.78±0.07	2.20±0.19	0.30±0.04
Heterozygote				
Male (n=8)	2.92±0.14	1.00±0.13	2.78±0.11	0.13±0.03
Female (n=10)	2.82±0.19	0.76±0.06	2.40±0.14	0.35±0.08
Homozygote				
Male (n=5)	4.53±0.35†	1.20±0.10	3.10±0.52	1.01±0.21†
Female (n=8)	4.64±0.68†	1.09±0.19	2.96±0.30*	1.46±0.44*

*$P<0.05$.
†$P<0.01$ vs wild type.

Lipid and Lipoprotein Profiles of *ARH* Knockout Mice

Table 1 shows total plasma cholesterol, triglycerides, LDL cholesterol, and HDL cholesterol levels of mice from litters derived from the mating of $ARH^{-/-}$ mice fed a normal chow. Plasma total cholesterol levels were 1.8-fold higher in $ARH^{-/-}$ mice than those in $ARH^{+/+}$. The elevation of total cholesterol was attributed to the six-fold increase of LDL cholesterol. There was no significant difference in the plasma cholesterol levels between $ARH^{-/-}$ and $ARH^{+/+}$ mice. Histological analysis of the liver showed that $ARH^{-/-}$ mice at 12 weeks of age did not have fatty livers, which were observed in our ARH patients.[5]

^{125}I-LDL Turnover Study

To investigate the LDL metabolism in ARH deficiency, ^{125}I-LDL turnover study was performed in $ARH^{-/-}$, $ARH^{+/-}$, $ARH^{+/+}$ (wild-type), and $LDLR^{-/-}$ mice. The clearance of ^{125}I-LDL from circulation is demonstrated in a semilogarithmic plot in Figure 2. It was substantially retarded in $ARH^{-/-}$ and $LDLR^{-/-}$ mice compared with wild-type mice. The clearance rate of ^{125}I-LDL in $ARH^{+/-}$ mice was similar to that in wild-type mice. The half-lives of the plasma ^{125}I-LDL were 11.7 hours in $ARH^{-/-}$ and 6.0 hours in $LDLR^{-/-}$ mice, and both were longer than those in $ARH^{+/-}$ and wild-type mice (2.8 hours).

Microscopic Findings in the Liver After Injection of DiI-LDL

To study whether the delayed clearance of LDL in $ARH^{-/-}$ mice is attributable to impaired catabolism of LDL in the liver, the liver specimen was examined after injection of DiI-LDL in wild-type, $LDLR^{-/-}$, and $ARH^{-/-}$ mice (Figure 3). Kupffer cells were identified by fluorescein isothiocyanate (Figure 3B, 3D, 3F, 3H, 3J, and 3L). Fluorescence activity was detected in the cytosol of the hepatocytes and Kupffer cells in wild-type mice, indicating that both types of cells effectively take-up DiI-LDL (Figure 3A). Pre-injection of 2.5 mg LDL raised serum total cholesterol from 2.18±0.66 (mean±SD) mmol/L to 14.67±0.68 mmol/L, and LDL cholesterol from 0.21±0.07 mmol/L to 11.42±1.09 mmol/L in wild-type mice (Table 2). In this condition, the incorporation

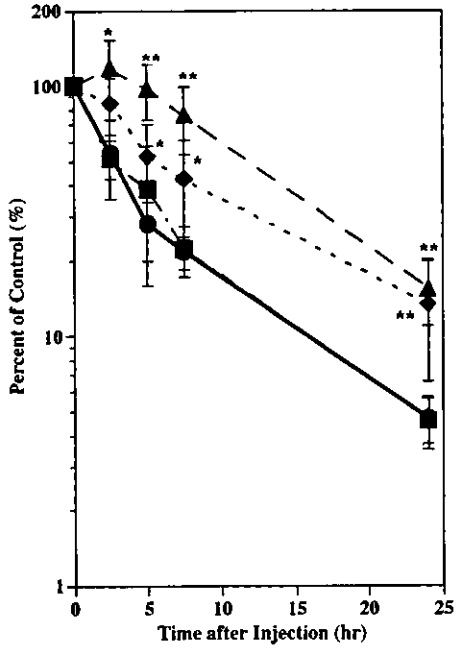

Figure 2. ^{125}I-LDL turnover study of wild-type (●), $ARH^{-/-}$ (■), $ARH^{+/-}$ (▲), and $LDLR^{-/-}$ (◆) mice. After 13 hours of fasting, wild-type, $ARH^{-/-}$, $ARH^{+/-}$, and $LDLR^{-/-}$ mice (three of each) were injected with 5 μg of ^{125}I-LDL. After the indicated time, blood was collected from the tail vein. The plasma content of ^{125}I-labeled apoB was measured by isopropanol precipitation, followed by gamma counting. The data are shown in semilogarithmic plots, and each data point represents the mean±SEM for triplicate assay. *$P<0.05$, **$P<0.01$.

of DiI-LDL into hepatocytes was decreased by the excess amount of LDL in plasma (Figure 3C), whereas its incorporation into Kupffer cells was not affected. In contrast, hepatocytes of $ARH^{-/-}$ mice were stained less extensively than those of wild-type mice by DiI-LDL fluorescence (Figure 3I), indicating that the uptake of DiI-LDL by the hepatocytes of $ARH^{-/-}$ mice was smaller than that of wild-type mice, and the presence of excess amount of LDL in plasma did not influence this result (Figure 3K). The fluorescence in the hepatocytes of $LDLR^{-/-}$ mice was also less intense than that in $ARH^{-/-}$ (Figure 3E).

In Vivo Hepatic Uptake of Intravenously Injected ^{3}H-CE-LDL

Hepatic uptake of LDL was also investigated by injecting ^{3}H-CE-LDL. Four hours after the injection, the tritium count in the blood decreased by 44% in wild-type mice, whereas it did not decrease in either $LDLR^{-/-}$ or $ARH^{-/-}$ mice (Figure 4A). The liver of wild-type mice incorporated 27.4±8.0% (mean±SD) of the injected ^{3}H-CE-LDL, whereas 9.0±1.0% was incorporated in $LDLR^{-/-}$ mice and 11.8±0.5% in $ARH^{-/-}$ mice (Figure 4B). The amount of ^{3}H-CE-LDL taken-up by the liver in $ARH^{-/-}$ was significantly smaller than that in wild-type mice but larger than that in $LDLR^{-/-}$ mice ($P<0.05$).

Incorporation of LDL in Primary Cultured Hepatocytes

In an attempt to reproduce the in vivo observations in vitro, incorporation of ^{3}H-CE-LDL was examined in primary cul-

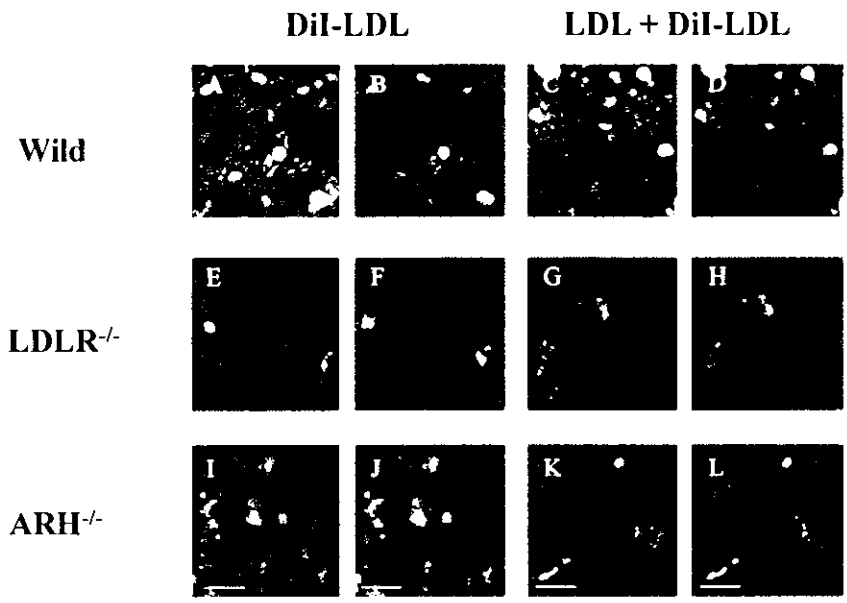

Figure 3. Microscopic findings of the liver after injection of DiI-LDL. A, E, and I, The liver from a mouse of each genotype 4 hours after the injection of 50 μg of DiI-LDL. C, G, and K, The liver from a mouse of each genotype, 4 hours after the injection of 2.5 mg of LDL, followed by 50 μg of DiI-LDL. B, F, and J, The liver from a mouse of each genotype, 4 hours after the injection of 50 μg of DiI-LDL. The specimens were stained with rat anti-mouse pan-macrophage antibody. D, H, and L, The liver from each genotype of mouse 4 hours after injection of 2.5 mg of LDL, followed by 50 μg of DiI-LDL. The specimen was stained with rat anti-mouse pan-macrophage antibody. The scale bar indicates 20 μm.

tured hepatocytes. Interestingly, the hepatocytes of *ARH*$^{-/-}$ mice internalized ^{3}H-CE-LDL as much as those of wild-type mice, whereas the hepatocytes of *LDLR*$^{-/-}$ mice took-up significantly less ^{3}H-CE-LDL (Figure 5A). The cultured hepatocytes of *ARH*$^{-/-}$ mice bound larger amounts of ^{125}I-LDL than those of wild-type and *LDLR*$^{-/-}$ mice. The hepatocytes of *ARH*$^{-/-}$ internalized and degraded ^{125}I-LDL as much as those of wild-type mice, which was significantly more than those of *LDLR*$^{-/-}$ mice (Figure 5B through 5D).

DiI-LDL Incorporation in Primary Cultured Hepatocytes

To confirm the positive incorporation of LDL by the primary cultured hepatocytes without ARH, the hepatocytes of *ARH*$^{-/-}$, *LDLR*$^{-/-}$, and wild-type mice were incubated with DiI-LDL and were observed by a laser confocal microscopy. Fluorescence-positive substances were observed in the cytosol of the hepatocytes of wild-type mice (Figure 6A), and they were suppressed in the presence of excess amounts of LDL (Figure 6B). The cultured hepatocytes of *LDLR*$^{-/-}$ mice showed very low fluorescence activity (Figure 6C and 6D). In contrast, the hepatocytes of *ARH*$^{-/-}$ mice showed fluorescence uptake of amounts similar to those observed for the wild-type (Figure 6E), and this was efficiently suppressed by excess amounts of LDL (Figure 6F).

TABLE 2. Cholesterol Levels of Total, VLDL, LDL, and HDL Fractions Before and After Administration of 2.5 mg LDL

	Total Cholesterol, mmol/L		VLDL Cholesterol, mmol/L		LDL Cholesterol, mmol/L		HDL Cholesterol, mmol/L	
	Before	After	Before	After	Before	After	Before	After
Wild-1	2.36	14.30	0.02	1.99	0.12	10.56	2.22	1.74
Wild-2	2.72	14.27	0.05	1.37	0.24	11.04	2.44	1.86
Wild-3	1.45	15.45	0.06	2.10	0.26	12.64	1.13	0.71
Mean	2.18	14.67	0.04	1.82	0.21	11.42	1.93	1.43
SD	0.66	0.68	0.02	0.39	0.07	1.09	0.70	0.63

VLDL indicates very-low-density lipoprotein.

Discussion

ARH knockout mice were developed by insertion mutation in the third intron of mouse chromosome 4. *ARH*$^{-/-}$ mice had a 1.8-fold higher plasma total cholesterol than wild-type litter mates fed normal chow, and this was attributed to a six-fold increase of LDL. Total cholesterol levels in *ARH*$^{-/-}$ mice (Table 1) were slightly lower than those reported for *LDLR*$^{-/-}$ mice (5.90±0.23 mmol/L in male, 6.18±0.21 mmol/L in female),[17] and cholesterol levels in *ARH*$^{+/-}$ mice (2.92±0.14 mmol/L in male, 2.82±0.19 mmol/L in female) were almost the same as those in *ARH*$^{+/+}$ mice (2.68±0.14 mmol/L in male, 2.57±0.22 mmol/L in female). The hypercholesterolemia in our *ARH*$^{-/-}$ mice appears to be milder than that reported by Jones et al,[14] who have recently reported that total cholesterol levels were moderately higher both in *ARH*$^{-/-}$ mice (7.96±1.63 mmol/L) and in *ARH*$^{+/-}$ mice (4.06±0.58 mmol/L) compared with that in *ARH*$^{+/+}$ mice (3.26±1.00 mmol/L) fed a chow containing 0.2% cholesterol. The difference in the plasma total cholesterol values between our *ARH*$^{-/-}$ mice and theirs may stem from different cholesterol content of the diet, because the chow we used contained 0.1% cholesterol.

The clearance of ^{125}I-LDL from the circulation was significantly delayed in *ARH*$^{-/-}$ mice like in *LDLR*$^{-/-}$ mice (Figure 2), indicating that the in vivo catabolic rate of LDL is decreased in *ARH*$^{-/-}$ mice. The half-life for the disappearance of ^{125}I-LDL in *ARH*$^{-/-}$ mice (11.7 hours) was longer than that observed in wild-type mice (2.8 hours) but not significantly different from that in *LDLR*$^{-/-}$ (6.0 hours). The LDL clearance in *ARH*$^{+/-}$ mice was same as that in the wild-type mice, suggesting that their LDL catabolism is normal. These results appear to be consistent with the findings in the ARH patients.[5]

To investigate the in vivo mechanism for the delayed catabolism of LDL directly in *ARH*$^{-/-}$ mice, hepatic uptake of

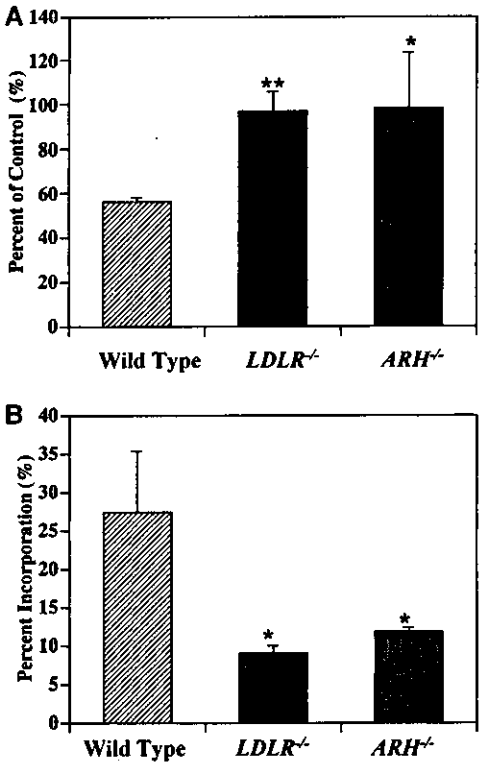

Figure 4. Hepatic uptake of intravenously injected ^{3}H-CE-LDL. ^{3}H-CE-LDL was injected into a mouse of each genotype. The blood was collected at 2 minutes and 4 hours after the injection. Immediately after the blood collection at 4 hours, 2 mg of LDL was injected and equilibrated for 10 minutes. The blood was washed from the body as described in the Methods section, and the liver was isolated. Lipid was extracted from the liver and the blood, and radioactivity was counted. Values are mean±SEM. A, Percentage of remaining tritium radioactivity in the mouse blood after 4 hours compared to that after 2 minutes. B, Hepatic uptake of tritium in the liver, 4 hours after injection, expressed as percentage of the total radioactivity injected calculated from the count in the blood at 2 minutes after the injection. *P<0.05, **P<0.01.

DiI-LDL was monitored. The fluorescence was recovered in the cytosols of both hepatocytes and Kupffer cells of wild-type mice (Figure 3A), and the fluorescence in the hepatocytes was suppressed by pretreatment with excess amounts of LDL (Figure 3C), suggesting that DiI-LDL was incorporated into the hepatocytes via the LDLR. Lower levels of DiI-LDL were found in hepatocytes of *LDLR*$^{-/-}$ and *ARH*$^{-/-}$ mice (Figure 3E, I). Because LDL cholesterol levels were higher in *ARH*$^{-/-}$ mice (1.01±0.21 mmol/L in male, 1.46±0.44 mmol/L in female) than that in wild-type mice (0.17±0.05 mmol/L in male, 0.30±0.04 mmol/L in female), injected DiI-LDL may become more diluted in *ARH*$^{-/-}$ by their own LDL. However, hepatic DiI-LDL uptake in *ARH*$^{-/-}$ mice was much lower than the observed uptake in wild-type mice when the excess LDL was given to raise LDL cholesterol (11.42±1.09 mmol/L). This indicates that the lower uptake of DiI-LDL in *ARH*$^{-/-}$ was not attributable to a dilution effect caused by their high LDL levels (Figure 3C, I).

Small numbers of cells appeared highly fluorescence-positive in the liver of mice of all the genotypes including *LDLR*$^{-/-}$ (Figure 3A, E, I). Their fluorescent activity was not

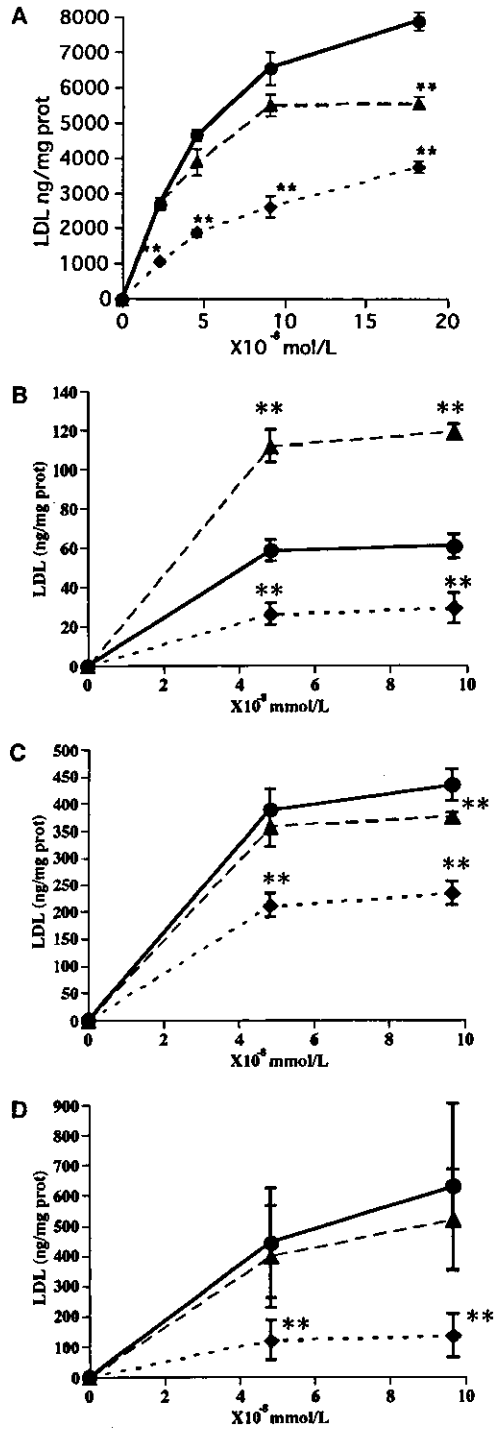

Figure 5. LDL receptor assay in primary cultured hepatocytes. Hepatocytes were obtained from the wild-type, *ARH*$^{-/-}$, and *LDLR*$^{-/-}$ mice, and cultured in Waymouth medium containing 10% fetal calf serum (day 0). On day 2, the medium was removed and the cells were washed twice. Then, the cells were cultured in Waymouth medium containing 10% LPDS. On day 3, the cells were subjected to LDL receptor assay. The data are shown as the mean±SEM of quadruplicate assays. The experiments were performed in the presence of 20-fold excess of LDL for nonspecific binding. A, ^{3}H-CE-LDL incorporation of primary cultured hepatocytes from wild-type (●), *LDLR*$^{-/-}$ (♦), and *ARH*$^{-/-}$ (▲) mice. *P<0.05, **P<0.01 vs wild-type. B, ^{125}I-LDL binding of primary cultured hepatocytes. C, ^{125}I-LDL incorporation of primary cultured hepatocytes. D, ^{125}I-LDL degradation of primary cultured hepatocytes.

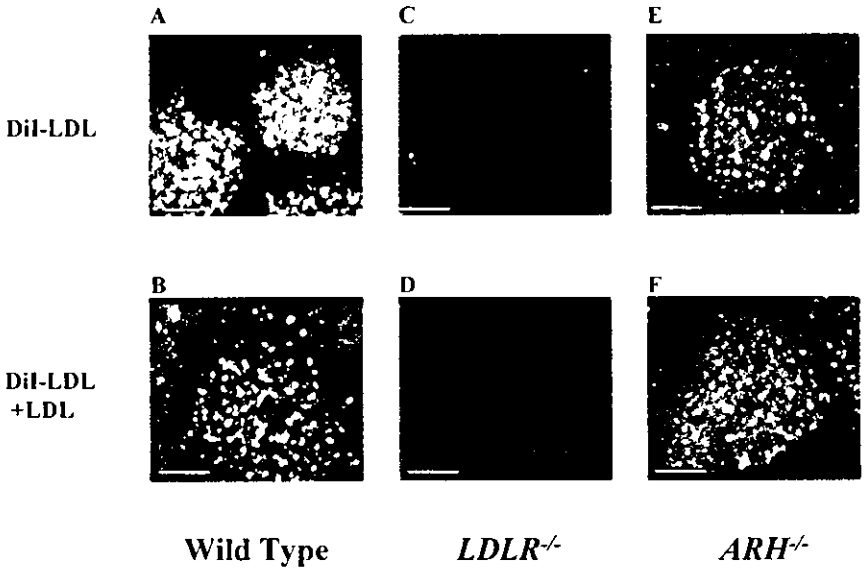

Figure 6. Dil-LDL incorporation in primary cultured hepatocytes of wild-type, $LDLR^{-/-}$, and $ARH^{-/-}$ mice. On day 0, hepatocytes were obtained from wild-type, $ARH^{-/-}$, and $LDLR^{-/-}$ mice, and cultured in Waymouth medium containing 10% fetal calf serum. After 4 hours, the cells were washed with PBS and cultured in Waymouth medium containing 10% LPDS. On day 2, the cells were incubated with Dil-LDL with or without 20 times excess of LDL for 3 hours. Then the cells were washed with PBS and mounted. A, C, and E, Hepatocytes from each genotype of mouse incubated with Dil-LDL. B, D, and F, Hepatocytes from each genotype of mouse incubated with Dil-LDL and excess of LDL. The scale bar indicates 10 μm.

decreased by the presence of excess amounts of LDL (Figure 3C, G, K) and these cells were positively identified as Kupffer cells by immunostaining with the antibody against mouse macrophages (Figure 3B, D, F, H, J, L). Thus, DiI-LDL was incorporated into Kupffer cells via an LDLR-independent pathway.

Hepatic uptake of LDL in $ARH^{-/-}$ was also examined by measuring the uptake of ^{3}H-CE-LDL by the liver. The tritium count in the blood decreased significantly in the wild-type mice, whereas it did not change in $LDLR^{-/-}$ and $ARH^{-/-}$ mice (Figure 4A). This is in agreement with the ^{125}I-LDL turnover study (Figure 2). The incorporation of ^{3}H-CE-LDL into the liver of $LDLR^{-/-}$ and $ARH^{-/-}$ mice was significantly lower than that of the wild-type mice (Figure 4B), suggesting again that the delayed turnover of LDL in $ARH^{-/-}$ mice is attributable to low LDL uptake by the liver. Interestingly, incorporation of ^{3}H-CE-LDL into the liver of $ARH^{-/-}$ is significantly higher than that of $LDLR^{-/-}$ ($P<0.05$). This result implies that the LDLR may function to incorporate LDL in the liver to some extent in vivo even without ARH.

To examine in vitro LDLR activity in the cells of $ARH^{-/-}$ mice, the incorporation of ^{3}H-CE-LDL was measured in primary cultured hepatocytes of $ARH^{-/-}$, $LDLR^{-/-}$, and wild-type mice (Figure 5A). The cultured hepatocytes of $ARH^{-/-}$ incorporated a slightly smaller amount of ^{3}H-CE-LDL than that of the wild-type, but much larger than that of $LDLR^{-/-}$. These findings were confirmed by ^{125}I-LDL incorporation and degradation experiments (Figure 5C, D). The binding of ^{125}I-LDL to the hepatocytes of $ARH^{-/-}$ was larger than that of wild-type (Figure 5B). Recently, Michaely et al[26] reported that the number of LDLRs on the cell surface of the lymphocytes in ARH subject was increased 20-fold, and that LDL binding activity was increased two-fold. The hepatocytes of $ARH^{-/-}$ seemed to remain the characteristics of in vivo status to some extent. To see whether LDL is incorporated into the cell or whether it remains on the cell surface, the cells were incubated with DiI-LDL and observed by using a laser confocal microscopy. The cytosol of the hepatocytes of $ARH^{-/-}$ mice was fluorescently stained, suggesting that DiI-LDL was internalized, like that of wild-type mice (Figure 6A, E). The results were highly consistent with the findings that the LDLR in the cultured fibroblasts from the homozygous ARH patients normally functioned, despite the fact that LDL clearance in their blood was severely impaired.[5] This suggests that the LDLR functions normally in vitro without ARH protein.

The PTB domain of ARH protein has been shown, by pull-down technique, to bind to the FDNPVY sequence of the LDLR protein.[8] ARH protein was also reported to interact with clathrin and AP-2, and it is suggested to function as an adaptor protein that couples LDLR to the endocytic machinery. ARH patients have severe hypercholesterolemia caused by delayed LDL clearance in vivo, although they have normal or subnormal levels of LDLR activity in their fibroblasts when measured in vitro.[5] However, transformed lymphocytes and monocyte-derived macrophages were unable to internalize LDL in ARH patients.[12] Thus, the dependency of LDLR function on ARH protein can be cell-specific. However, we have demonstrated here that hepatocytes do not take-up LDL in vivo without ARH protein, but they normally catabolize LDL in vitro. Thus, the requirement of ARH protein for proper functioning of the LDLR is not cell-specific, but rather may depend on the cellular environment.

Hepatic uptake of ^{3}H-CE from LDL was shown to be significantly higher in $ARH^{-/-}$ mice than $LDLR^{-/-}$ mice. This may indicate that LDLR functions to some extent without ARH, even in vivo. Some other adaptor proteins may compensate for ARH by forming an LDLR–clathrin complex, or the condition can be induced so LDLRs can be internalized without forming a clathrin complex. Our in vitro results strongly indicate that these possibilities may be enabled in a certain cellular environments.

Acknowledgments

This work was supported in part by the Promotion of Fundamental Studies in Health Science of the Organization for Pharmaceutical Safety and Research (OPSR); Research on Advanced Medical Technology from the Ministry of Health, Labour, and Welfare; Ono Medical Research Foundation; Takeda Medical Research Founda-

tion; and grant-in-aid for Scientific Research (C) (No. 15590964) from the Ministry of Education, Science, Sports, and Culture, Japan. We thank Drs Kenji Kangawa, Hisayuki Matsuo, and Hitonobu Tomoike for their helpful discussion and advice, Dr Michitaka Masuda for taking the photograph, and Dr Patrick Leahy for proofreading this manuscript. We also thank Moto Ohira, Eri Abe, Ritsuko Maeda, and Keiko Jinno for their excellent technical assistance.

References

1. Khachadurian AK, Uthman SM. Experiences with the homozygous cases of familial hypercholesterolemia. A report of 52 patients. *Nutr Metab.* 1973;15:132–140.
2. Brown MS, Anderson RG, Basu SK, Goldstein JL. Recycling of cell-surface receptors: observations from the LDL receptor system. *Cold Spring Harb Symp Quant Biol.* 1982;46(Pt 2):713–721.
3. Goldstein JL, Hobbs HH, Brown MS. Familial hypercholesterolemia. In: Scriver CR, Beaudet AL, Sly WS, Valle D, eds. *The Metabolic and Molecular Bases of Inherited Disease.* 8th ed., Vol II. New York: McGraw-Hill; 2001:2863–2913.
4. Harada-Shiba M, Tajima S, Miyake Y, Kojima S, Tsushima M, Yamamoto A. Severe hypercholesterolemia patients with normal LDL receptor. *J Jpn Atheroscler Soc.* 1991;19:227–242.
5. Harada-Shiba M, Tajima S, Yokoyama S, Miyake Y, Kojima S, Tsushima M, Kawakami M, Yamamoto A. Siblings with normal LDL receptor activity and severe hypercholesterolemia. *Arterioscler Thromb.* 1992;12:1071–1078.
6. Garcia CK, Wilund K, Arca M, Zuliani G, Fellin R, Maioli M, Calandra S, Bertolini S, Cossu F, Grishin N, Barnes R, Cohen JC, Hobbs HH. Autosomal recessive hypercholesterolemia caused by mutations in a putative LDLR adaptor protein. *Science.* 2001;292:1394–1398.
7. Harada-Shiba M, Takagi A, Miyamoto Y, Tsushima M, Ikeda Y, Yokoyama S, Yamamoto A. Clinical features and genetic analysis of autosomal recessive hypercholesterolemia. *J Clin Endocrinol Metab.* 2003;88:2541–2547.
8. He G, Gupta S, Yi M, Michaely P, Hobbs HH, Cohen JC. ARH is a modular adaptor protein that interacts with the LDL receptor, clathrin, and AP-2. *J Biol Chem.* 2002;277:44044–44049.
9. Schmidt HH, Stuhrmann M, Shamburek R, Schewe CK, Ebhardt M, Zech LA, Buttner C, Wendt M, Beisiegel U, Brewer HB, Jr, Manns MP. Delayed low density lipoprotein (LDL) catabolism despite a functional intact LDL-apolipoprotein B particle and LDL-receptor in a subject with clinical homozygous familial hypercholesterolemia. *J Clin Endocrinol Metab.* 1998;83:2167–2174.
10. Zuliani G, Arca M, Signore A, Bader G, Fazio S, Chianelli M, Bellosta S, Campagna F, Montali A, Maioli M, Pacifico A, Ricci G, Fellin R. Characterization of a new form of inherited hypercholesterolemia: familial recessive hypercholesterolemia. *Arterioscler Thromb Vasc Biol.* 1999;19:802–809.
11. Zuliani G, Vigna GB, Corsini A, Maioli M, Romagnoni F, Fellin R. Severe hypercholesterolaemia: unusual inheritance in an Italian pedigree. *Eur J Clin Invest.* 1995;25:322–331.
12. Norman D, Sun XM, Bourbon M, Knight BL, Naoumova RP, Soutar AK. Characterization of a novel cellular defect in patients with phenotypic homozygous familial hypercholesterolemia. *J Clin Invest.* 1999;104:619–628.
13. Eden ER, Patel DD, Sun XM, Burden JJ, Themis M, Edwards M, Lee P, Neuwirth C, Naoumova RP, Soutar AK. Restoration of LDL receptor function in cells from patients with autosomal recessive hypercholesterolemia by retroviral expression of ARH1. *J Clin Invest.* 2002;110:1695–1702.
14. Jones C, Hammer RE, Li WP, Cohen JC, Hobbs HH, Herz J. Normal sorting but defective endocytosis of the low density lipoprotein receptor in mice with autosomal recessive hypercholesterolemia. *J Biol Chem.* 2003;278:29024–29030.
15. Usui S, Hara Y, Hosaki S, Okazaki M. A new on-line dual enzymatic method for simultaneous quantification of cholesterol and triglycerides in lipoproteins by HPLC. *J Lipid Res.* 2002;43:805–814.
16. Zambrowicz BP, Friedrich GA, Buxton EC, Lilleberg SL, Person C, Sands AT. Disruption and sequence identification of 2,000 genes in mouse embryonic stem cells. *Nature.* 1998;392:608–611.
17. Ishibashi S, Brown MS, Goldstein JL, Gerard RD, Hammer RE, Herz J. Hypercholesterolemia in low density lipoprotein receptor knockout mice and its reversal by adenovirus-mediated gene delivery. *J Clin Invest.* 1993;92:883–893.
18. Sambrook J, Russell DW. *Molecular Cloning: A Laboratory Manual.* Cold Spring Harbor: Cold Spring Harbor Laboratory Press; 2001.
19. Nishimura N, Harada-Shiba M, Tajima S, Sugano R, Yamamura T, Qiang QZ, Yamamoto A. Acquisition of secretion of transforming growth factor-beta 1 leads to autonomous suppression of scavenger receptor activity in a monocyte-macrophage cell line, THP-1. *J Biol Chem.* 1998;273:1562–1567.
20. Bilheimer DW, Eisenberg S, Levy RI. The metabolism of very low density lipoprotein proteins. I. Preliminary in vitro and in vivo observations. *Biochim Biophys Acta.* 1972;260:212–221.
21. Nishikawa O, Yokoyama S, Okabe H, Yamamoto A. Enhancement of non-polar lipid transfer reaction through stabilization of substrate lipid particles with apolipoproteins. *J Biochem (Tokyo).* 1988;103:188–194.
22. Folch J, Lees M, Sloane Stanley GH. A simple method for the isolation and purification of total lipides from animal tissues. *J Biol Chem.* 1957;226:497–509.
23. Seglen PO. Control of glycogen metabolism in isolated rat liver cells by glucose, insulin and glucagon. *Acta Endocrinol Suppl (Copenh).* 1974;191:153–158.
24. Hara H, Yokoyama S. Interaction of free apolipoproteins with macrophages. Formation of high density lipoprotein-like lipoproteins and reduction of cellular cholesterol. *J Biol Chem.* 1991;266:3080–3086.
25. Goldstein JL, Basu SK, Brown MS. Receptor-mediated endocytosis of low-density lipoprotein in cultured cells. *Methods Enzymol.* 1983;98:241–260.
26. Michaely P, Li WP, Anderson RG, Cohen JC, Hobbs HH. The modular adaptor protein ARH is required for low density lipoprotein (LDL) binding and internalization but not for LDL receptor clustering in coated pits. *J Biol Chem.* 2004;279:34023–34031.

Adrenomedullin Gene Transfer Induces Therapeutic Angiogenesis in a Rabbit Model of Chronic Hind Limb Ischemia

Benefits of a Novel Nonviral Vector, Gelatin

Noriyuki Tokunaga, MD; Noritoshi Nagaya, MD; Mikiyasu Shirai, MD; Etsuro Tanaka, MD; Hatsue Ishibashi-Ueda, MD; Mariko Harada-Shiba, MD; Munetake Kanda, MD; Takefumi Ito, MD; Wataru Shimizu, MD; Yasuhiko Tabata, PhD; Masaaki Uematsu, MD; Kazuhiro Nishigami, MD; Shunji Sano, MD; Kenji Kangawa, PhD; Hidezo Mori, MD

Background—Earlier studies have shown that adrenomedullin (AM), a potent vasodilator peptide, has a variety of cardiovascular effects. However, whether AM has angiogenic potential remains unknown. This study investigated whether AM gene transfer induces therapeutic angiogenesis in chronic hind limb ischemia.

Methods and Results—Ischemia was induced in the hind limb of 21 Japanese White rabbits. Positively charged biodegradable gelatin was used to produce ionically linked DNA-gelatin complexes that could delay DNA degradation. Human AM DNA (naked AM group), AM DNA-gelatin complex (AM-gelatin group), or gelatin alone (control group) was injected into the ischemic thigh muscles. Four weeks after gene transfer, significant improvements in collateral formation and hind limb perfusion were observed in the naked AM group and AM-gelatin group compared with the control group (calf blood pressure ratio: 0.60±0.02, 0.72±0.03, 0.42±0.06, respectively). Interestingly, hind limb perfusion and capillary density of ischemic muscles were highest in the AM-gelatin group, which revealed the highest content of AM in the muscles among the three groups. As a result, necrosis of lower hind limb and thigh muscles was minimal in the AM-gelatin group.

Conclusions—AM gene transfer induced therapeutic angiogenesis in a rabbit model of chronic hind limb ischemia. Furthermore, the use of biodegradable gelatin as a nonviral vector augmented AM expression and thereby enhanced the therapeutic effects of AM gene transfer. Thus, gelatin-mediated AM gene transfer may be a new therapeutic strategy for the treatment of peripheral vascular diseases. (***Circulation.*** **2004;109:526-531.)**

Key Words: peripheral vascular disease ■ angiogenesis ■ gene therapy ■ ischemia

Adrenomedullin (AM) is a potent vasodilator peptide that was originally isolated from human pheochromocytoma.[1] AM and its receptor are expressed mainly in vascular endothelial cells and vascular smooth muscle cells.[2–4] AM not only induces vasorelaxation but also regulates growth and death of these vascular cells.[5–10] These findings suggest that AM plays an important role in maintaining vascular homeostasis in an autocrine and/or paracrine manner.

A recent study has shown that vascular abnormalities are present in homozygous AM knockout mice, suggesting that AM is indispensable for vascular morphogenesis.[11–13] More recently, AM has been shown to activate the PI3K/Akt-dependent pathway in vascular endothelial cells, which is considered to regulate multiple critical steps in angiogenesis, including endothelial cell survival, proliferation, migration, and capillary-like structure formation.[7,14] These results raise the possibility that AM plays a role in modulating vasculogenesis and angiogenesis. However, whether AM induces therapeutic angiogenesis remains unknown.

Received May 20, 2003; revision received September 25, 2003; accepted September 26, 2003.

From the Department of Cardiac Physiology, National Cardiovascular Center Research Institute, Osaka, Japan (N.T., M.S., M.K., H.M.); the Department of Cardiovascular Surgery, Okayama University Medical School, Okayama, Japan (N.T., S.S.); the Department of Regenerative Medicine and Tissue Engineering, National Cardiovascular Center Research Institute, Osaka, Japan (N.N., T.I.); the Department of Internal Medicine, National Cardiovascular Center, Osaka, Japan (N.N., W.S., K.N.); the Department of Physiology, the Research Center for Genetic Engineering and Cell Transplantation, Tokai University School of Medicine, Isehara, Japan (E.T.); the Department of Pathology, National Cardiovascular Center, Osaka, Japan (H.I.-U.); the Department of Biochemistry, National Cardiovascular Center Research Institute, Osaka, Japan (M.H.-S., K.K.); the Department of Biomaterials, Field of Tissue Engineering, Institute for Frontier Medical Sciences, Kyoto University, Kyoto, Japan (Y.T.); and the Cardiovascular Division, Kansai Rosai Hospital, Hyogo, Japan (M.U.).

Correspondence to Noritoshi Nagaya, MD, Department of Regenerative Medicine and Tissue Engineering or Hidezo Mori, MD, Department of Cardiac Physiology, National Cardiovascular Center Research Institute, 5-7-1 Fujishirodai, Suita, Osaka 565-8565, Japan. E-mail nagayann@hsp.ncvc.go.jp or hidemori@ri.ncvc.go.jp

Circulation is available at http://www.circulationaha.org

DOI: 10.1161/01.CIR.0000109700.81266.32

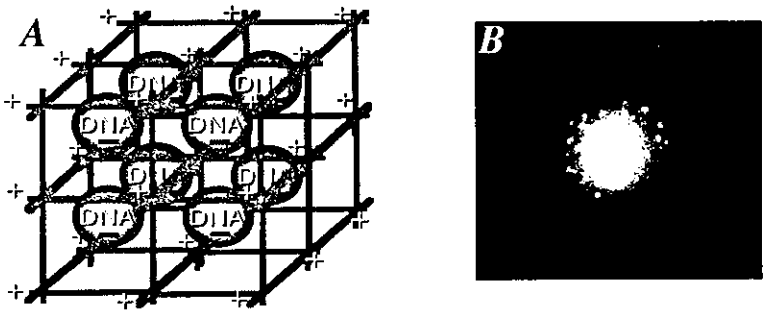

Figure 1. A, Schema of DNA-gelatin complex. Biodegradable gelatin can hold negatively charged plasmid DNA in its positively charged lattice structure. B, RITC-labeled AM DNA particles were incorporated into gelatin.

We prepared biodegradable gelatin that could hold negatively charged protein or plasmid DNA in its positively charged lattice structure.[15,16] Biodegradable gelatin has been widely used as a carrier of protein because of its capacity to delay protein degradation.[15] Similarly, ionically linked DNA-gelatin complexes can delay gene degradation.[16] These findings raise the possibility that gelatin may serve as a nonviral vector for gene therapy.

Thus, the purposes of this study were (1) to investigate whether AM gene transfer induces therapeutic angiogenesis in a rabbit model of chronic hind limb ischemia and (2) to examine whether the use of biodegradable gelatin as a vector augments AM expression and thereby enhances the therapeutic effects of AM gene transfer.

Methods

Animal Model

All protocols were performed in accordance with the guidelines of the Animal Care Ethics Committee of the National Cardiovascular Center Research Institute. Twenty-one male Japanese White rabbits (body weight, 2.9±0.1 kg; Japan Animal Co, Osaka, Japan) were used for physiological and morphological assessment. In addition, 30 rabbits were used for radioimmunoassay, immunohistochemical examination, and Western blot analysis. After anesthetization with pentobarbital sodium (30 to 35 mg/kg), a longitudinal incision was made in the left thigh, extending inferiorly from the inguinal ligament to a point just proximal to the patella. Hind limb ischemia was induced by ligation of the distal left external iliac artery and complete resection of the left femoral artery, as described previously.[17]

Construction of Plasmid DNA

To construct the expression vector for human AM, the *EcoRI/XhoI* fragment of the full-length human AM cDNA was ligated into the EcoRI/XhoI fragment of the pcDNA1.1-CMV expression plasmid (Invitrogen). To verify that the pcDNA1.1-CMV vector encoding AM cDNA produces a biologically active AM protein, the expression vector was transfected into 293 cells, and AM activity in the transfected cells was measured by high-performance liquid chromatography and radioimmunoassay. The pcDNA1.1-CMV vector encoding β-galactosidase (LacZ) cDNA was used as a control DNA.

Preparation of AM DNA-Gelatin Complex

Biodegradable gelatin was prepared from pig skin. The gelatin was characterized by a spheroid shape with a diameter of approximately 30 μm, water content of 95%, and an isoelectric point (pI) of 9 after swelling in water.[15,16] Gelatin can hold negatively charged protein or plasmid DNA in its positively charged lattice structure (Figure 1A). Dried gelatin (4 mg, pI 9) was added to human AM DNA solution (500 μg/100 μL in phosphate-buffered saline, pH 7.4). After mixture of DNA and gelatin, DNA-gelatin complexes were incubated at 37 °C for 2 hours.

To visualize incorporation of DNA into gelatin, AM plasmid DNA was labeled with rhodamine B isothiocyanate (RITC), as reported previously.[16] In brief, the coupling reaction of RITC to plasmid DNA was carried out by mixing the two substances in 0.2 mol/L sodium carbonate-buffered solution (pH 9.7), followed by gel filtration with a PD 10 column (Amersham-Pharmacia). RITC-labeled AM DNA was incorporated into positively charged gelatin (Figure 1B).

Study Protocol

Ten days after the induction of hind limb ischemia (day 10), AM DNA (naked AM group, n=7), AM DNA-gelatin complex (AM-gelatin group, n=7), or gelatin alone (control group, n=7) was administered intramuscularly into 3 different sites in the ischemic adductor muscle and 2 different sites in the semimembranous muscle. In addition, Lac Z DNA-gelatin complex served as a control DNA (Lac Z-gelatin group, n=5). The amount of plasmid was 500 μg (1 mL) and that of gelatin was 4 mg. Morphological and angiographic analyses and measurements of calf blood pressure and laser Doppler flow were performed 4 weeks after gene transfer (day 38). After completion of these measurements, the adductor, semimembranous, and gastrocnemius muscles were weighed in each hind limb.[18] The muscle weight ratio was calculated for each muscle as follows: muscle weight ratio=muscle weight in ischemic hind limb/muscle weight in nonischemic hind limb. Specimens of the adductor muscle of the ischemic hind limb were obtained for histological examination.

Measurement of Calf Blood Pressure

Calf blood pressure was measured on days 10 and 38 in both hind limbs with a Doppler flowmeter (Hayashi Denki Co, Ltd) and a 25-mm-wide cuff. The pulse of the posterior tibial artery was identified with the use of a Doppler probe, and the systolic blood pressure in both hind limbs was determined by standard techniques. The calf blood pressure ratio was defined for each rabbit as the ratio of systolic pressure of the ischemic hind limb to that of the normal hind limb.[17]

Laser Doppler Blood Perfusion Analysis

Blood flow of the ischemic hind limb was measured with the use of a laser Doppler blood perfusion image system (moorLDI, Moor Instruments) on day 38.

Angiographic Analysis

Development of collateral arteries was evaluated by angiography on days 0 and 38. A 4F catheter was placed in the left internal iliac artery through the common carotid artery, and 3 mL contrast medium (Iopamiron 300, SCHERING) was injected with an automated angiography injector at a rate of 2.5 mL/s. Quantitative angiographic analysis of collateral vessel development in the ischemic hind limb was performed with the use of a 5-mm^2 grid overlay, as described previously.[17] The angiographic score was calculated for each film as the ratio of grid intersections crossed by opacified arteries divided by the total number of grid intersections in the ischemic medial thigh. The angiographic score was determined by 2 blinded observers.

Morphological and Histological Examination

The degree of lower hind limb necrosis and thigh muscle necrosis was macroscopically evaluated on graded morphological scales (grade 1 to 3) for peripheral tissue damage and muscle necrosis area of the adductor, semimembranous, and medial large muscles. Capillary density of the ischemic hind limb was evaluated by alkaline phosphatase staining, as reported previously.[17] A total of 10 different fields from three different sections were randomly selected, and the number of capillaries was counted under a ×40 objective. Capillary density was expressed as the mean number of capillaries per square millimeter. The number of myofibers in each field was also examined and the capillary/muscle fiber ratio calculated.

Radioimmunoassay for Human AM

Human AM production was examined 1, 2, and 4 weeks after gene transfer in the naked AM group, AM-gelatin group, and control group (n=5 each). The muscles were harvested for radioimmunoassay and immunohistochemical examination. Immunoreactive human AM level in rabbit muscles was determined by immunoradiometric assay with the use of a specific kit (Shionogi Co, Ltd).[19] Tissue content of vascular endothelial growth factor (VEGF) was examined by ELISA kit (R&D systems).

Immunohistochemistry for Human AM, Ki67 Antigen, and Phosphorylated Akt

Immunohistochemical studies were performed on formalin-fixed, paraffin-embedded 4-μm sections of ischemic thigh muscles 7 days after gene transfer. To elucidate AM expression after gene therapy, immunohistochemistry for human AM was performed with the use of a monoclonal antibody recognizing AM-(12–25) (1:100), as reported previously.[20] To evaluate the proliferative potential of AM, tissue sections were stained for Ki67, a marker for cell proliferation, with the use of monoclonal anti-Ki67 antibody (1:100) (DAKO). AM has recently been shown to promote proliferation of vascular endothelial cells at least in part through the PI3k/Akt pathway.[21] Thus, immunohistochemistry for phosphorylated Akt was performed with mouse monoclonal anti-phosphorylated Akt antibody (1:100) (Cell Signaling Technology).

Western Blot Analysis

To identify Akt phosphorylation in ischemic muscles after AM gene transfer, Western blotting was performed with the use of a commercially available kit (PhosphoPlus Akt [Ser473] Antibody Kit, Cell Signaling Technology). Ischemic muscles in the 3 groups were obtained 7 days after AM gene transfer. These samples were homogenized on ice in 0.1% Tween 20 homogenization buffer with a protease inhibitor (Complete, Roche). After centrifugation for 20 minutes at 4°C, the supernatant was used for Western blot analysis. The 50 μg of protein was transferred into sample buffer, loaded on 7.5% SDS-polyacrylamide gel, and blotted onto nitrocellulose membrane through the use of a wet blotting system. After blocking for 60 minutes, the membranes were incubated with primary antibodies (1:500) at 4°C overnight. The membranes were then incubated with secondary antibodies, which were conjugated with horseradish peroxidase (Cell Signaling Technology), at a final dilution of 1:2000. Signals were detected through the use of LumiGLO chemiluminescence reagents (Cell Signaling Technology).

Statistical Analysis

All results are expressed as mean±SEM. Statistical significance was evaluated by 1-way ANOVA followed by Fisher's analysis, Scheffe's F analysis, or Kruskal-Wallis test. A value of $P<0.05$ was considered statistically significant.

Results

Physiological and Morphological Assessment

Complete resection of the left femoral artery resulted in a similar decrease in calf blood pressure ratio among the 3 groups before the initiation of therapy (day 10) (Figure 2A). However, the calf blood pressure ratio on day 38 was highest in the AM-gelatin groups, followed by the naked AM group and subsequently the control group. The laser Doppler flow in hind limb was highest in the AM-gelatin group, followed by the naked AM group and the control group (Figure 2B). The calf blood pressure ratio and laser Doppler flow 4 weeks after gene transfer did not significantly differ between the control group and Lac Z-gelatin group. Lower hind limb necrosis was minimal in the AM-gelatin group, followed by the naked AM group and the control group (Figure 2C). Thigh muscle necrosis was also minimal in the AM-gelatin group. Similarly, the muscle weight ratio (ischemic/normal) on day 38 was highest in the AM-gelatin group (Table). Neither mean arterial pressure nor heart rate significantly differed among the 3 groups.

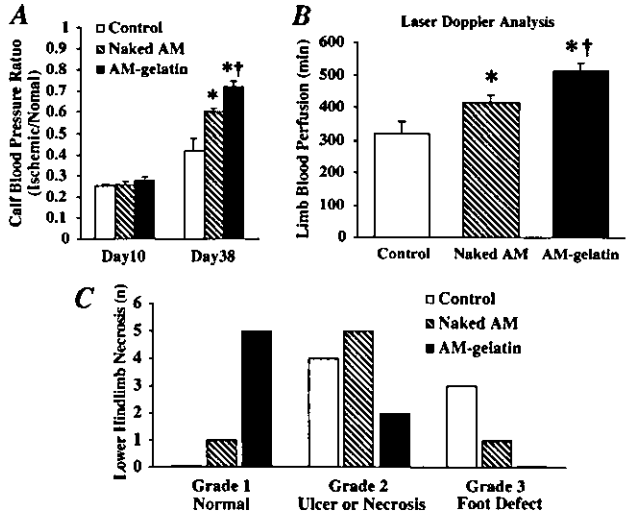

Figure 2. A, Calf blood pressure ratio (ischemic/normal hind limb) before (on day 10) and after (on day 38) gene transfer. B, Measurement of laser Doppler flow on day 38. Data are mean±SEM. *$P<0.05$ vs control group; †$P<0.05$ vs naked AM group. C, Number of cases of each grade of lower hind limb necrosis on day 38. Lower hind limb necrosis was minimal in the AM-gelatin group. Number of necrosis or foot defect is statistically significant among the 3 groups ($P<0.05$ by Kruskal-Wallis test).

Angiographic Analysis

Angiograms 4 weeks after gene transfer (day 38) showed the development of collateral arteries in the naked AM and

Physiological Characteristics

	Control	Naked AM	AM-Gelatin
No. of rabbits	7	7	7
Body weight, kg	2.46±0.06	2.65±0.10	3.16±0.09
MAP, mm Hg	112±3	114±3	116±2
HR, beats/min	269±12	253±5	262±7
Muscle weight ratio	0.71±0.03	0.84±0.02*	0.95±0.02*†

MAP indicates mean arterial pressure; HR, heart rate; and muscle weight ratio, ratio of muscle weight in ischemic hind limb to that in nonischemic hind limb. Data are mean±SEM.

*$P<0.01$ vs control group; †$P<0.05$ vs naked AM group.

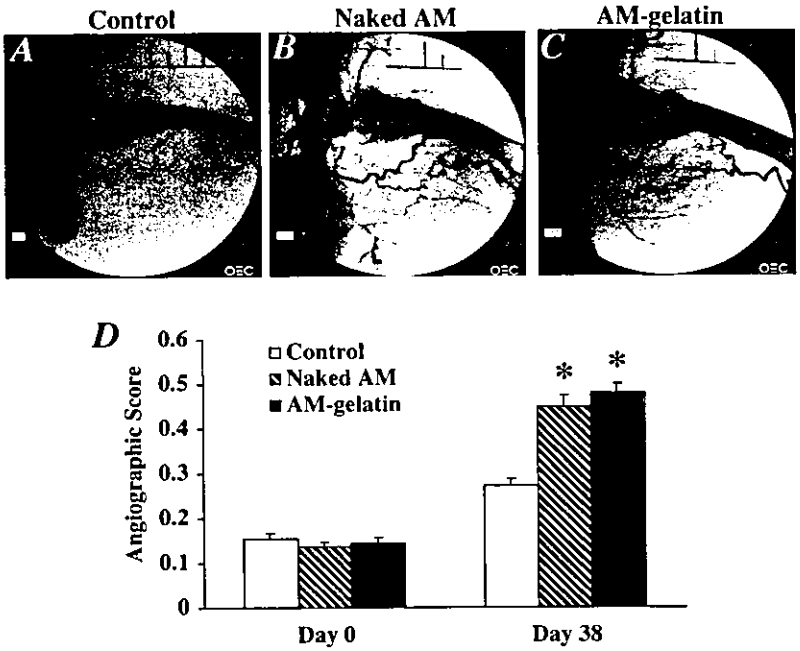

Figure 3. Representative angiograms of control group (A), naked AM group (B), and AM-gelatin group (C) on day 38. Collateral arteries were well developed in the naked AM and AM-gelatin groups. D, Angiographic score on days 0 and 38 in each group. Angiographic score on day 38 was significantly higher in the naked AM and AM-gelatin groups than in the control group. Data are mean±SEM. *$P<0.001$ versus control group.

AM-gelatin groups compared with that in the control group (Figure 3, A through C). Quantitative analysis of collateral vessels demonstrated that the angiographic score in both the naked AM and AM-gelatin groups was significantly higher than that in the control group (Figure 3D). Angiographic score did not significantly differ between the control group and Lac Z-gelatin group.

To examine the development of collateral vessels in an earlier stage, other rabbits (n=4 each) were examined 2 weeks after gene transfer (day 24). Angiograms showed significant collateral development in the naked AM and AM-gelatin groups compared with that in the control group.

Histological Examination

Alkaline phosphatase staining of ischemic hind limb muscle showed marked augmentation of neovascularization in both the naked AM and AM-gelatin groups compared with the control group (Figure 4, A through C). Quantitative analysis demonstrated that capillary density of the ischemic adductor muscle was highest in the AM-gelatin group (Figure 4D). Analysis of the capillary/muscle fiber ratio yielded similar results. Seven days after gene transfer, intense immunostaining for Ki67 was observed in vascular endothelial cells of the naked AM and the AM-gelatin groups (Figure 4, E through G).

AM Expression and Akt Phosphorylation After Gene Transfer

Seven days after gene transfer, modest immunostaining for human AM was observed in the naked AM group, whereas AM immunoreactivity was intense surrounding the gelatin in the AM-gelatin group (Figure 5, A through C). Tissue content of human AM was significantly increased both in the naked AM and the AM-gelatin groups 7 days after gene transfer (Figure 5D). The AM level in the AM-gelatin group was significantly higher that in the naked AM group. Two weeks after gene transfer, AM overexpression was observed only in the AM-gelatin group. The expression of endogenous VEGF and its receptors (Flt-1 and Flk-1) did not differ among the 3 groups (data not shown). Western blot analysis revealed that phosphorylated Akt in ischemic muscles was increased in both the naked AM and AM-gelatin groups 7 days after gene transfer (Figure 5E). Intense immunostaining for phosphory-

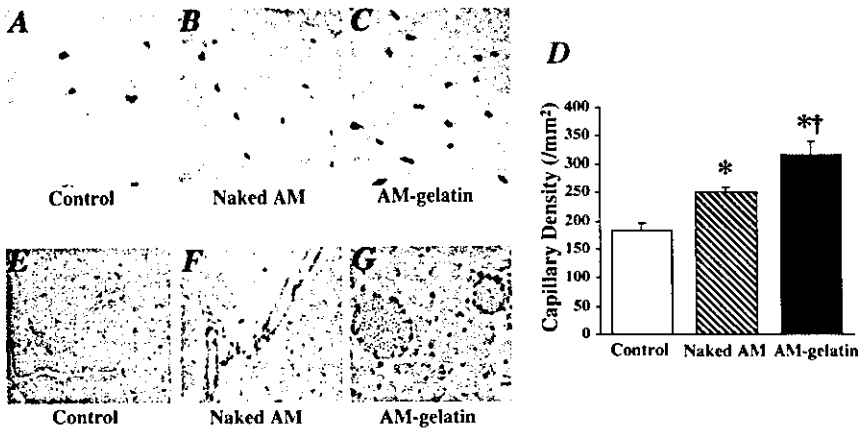

Figure 4. A through C, Representative examples of alkaline phosphatase staining in ischemic hind limb muscles. Magnification ×200. D, Quantitative analysis of capillary density in ischemic hind limb muscles. Data are mean±SEM. *$P<0.05$ vs control group; †$P<0.05$ vs naked AM group. E through G, Immunohistochemical analysis of Ki67 antigen, a marker for cell proliferation. Magnification ×400.

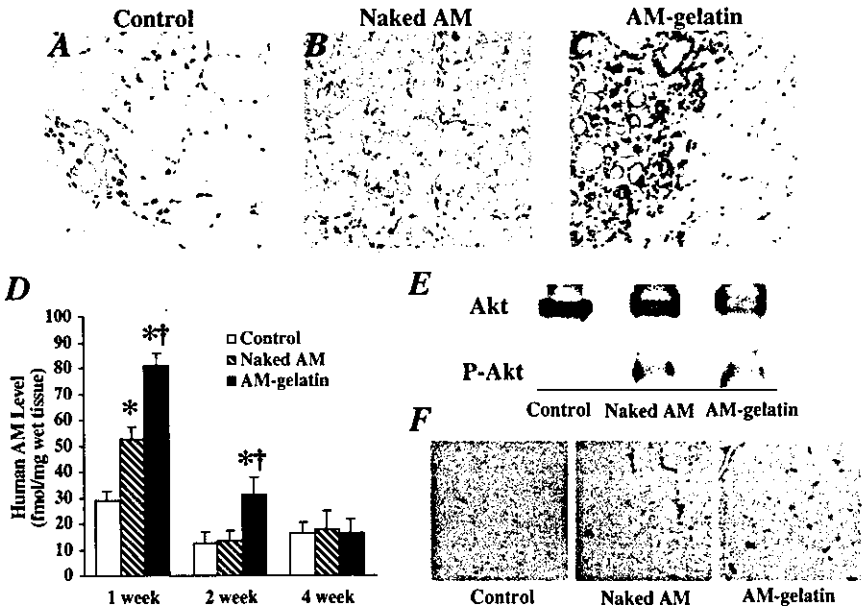

Figure 5. A through C, Immunohistochemistry for human AM 7 days after gene transfer. Intense immunostaining was observed surrounding gelatin in the AM-gelatin group. Magnification ×200. D, Time course of AM production in ischemic muscles after gene transfer. Data are mean±SEM. *$P<0.01$ vs control group; †$P<0.01$ vs naked AM group. E, Western blot analysis for Akt phosphorylation in muscles. F, Immunohistochemical staining for phosphorylated Akt 7 days after gene transfer. Phosphorylated Akt was distributed at least in endothelial cells. Magnification ×400.

lated Akt was observed at least in endothelial cells of the Naked AM and the AM-gelatin groups (Figure 5F).

Discussion

We demonstrated that (1) AM gene transfer induced hemodynamic and angiographic improvements in association with an increase in capillary density in a rabbit model of chronic hind limb ischemia. We also demonstrated that (2) administration of AM DNA-gelatin complexes markedly augmented AM expression and thereby enhanced the therapeutic effects of AM gene transfer.

AM has a variety of effects on the vasculature that include vasodilation,[1,5–7] inhibition of endothelial cell apoptosis,[8,9] and regulation of smooth muscle cell proliferation.[10] However, whether AM has angiogenic potential has remained unknown. In the present study, intramuscular administration of naked AM DNA augmented AM production in skeletal muscles, as indicated by increased tissue content and significant immunostaining of AM. As a result, AM gene transfer increased hind limb perfusion and ameliorated lower hind limb and thigh muscle necrosis in a rabbit model of hind limb ischemia. AM gene transfer may protect the ischemic hind limb partly by improving the blood flow in the ischemic hind limb because AM is originally identified as a potent vasodilating peptide.[1] Nevertheless, angiographic collateral development and high capillary density were observed in ischemic muscles after AM gene transfer. Ki67, a marker for cell proliferation, was detected in endothelial cells of microvessels after AM gene transfer. These results suggest that AM overproduction resulting from gene transfer may induce angiogenesis in a rabbit model of hind limb ischemia. Recent studies using AM gene knockout mice have shown that AM is essential for development of the vasculature during embryogenesis.[11–13] These studies support our results that AM may be an angiogenic factor. VEGF is known to induce angiogenesis and to regulate endothelial cell survival through the phosphatidylinositol 3-kinase (PI3K)/Akt pathway.[22] Thus, the PI3K/Akt pathway is considered to regulate multiple critical steps in angiogenesis, including endothelial cell survival, proliferation, migration, and capillary-like structure formation.[14] A recent study has reported that AM promotes proliferation and migration of human umbilical vein endothelial cells at least in part through the PI3K/Akt pathway.[21] The present study demonstrated that phosphorylated Akt is increased at least in endothelial cells after AM gene transfer. AM gene transfer did not influence endogenous VEGF and its receptors. Taken together, it is interesting to speculate that AM may directly induce angiogenesis through the PI3K/Akt pathway.

In the present study, we used positively charged biodegradable gelatin as a nonviral vector. We have shown that basic fibroblast growth factor (bFGF) is ionically linked with gelatin, which enhances the angiogenic effects of bFGF by delaying protein degradation.[15] Thus, biodegradable gelatin has been used as a carrier of protein. However, little information is available regarding the therapeutic potential of gelatin as a nonviral vector for gene transfer. In the present study, we demonstrated that RITC-labeled AM DNA was incorporated into positively charged gelatin. In addition, intramuscular administration of AM DNA-gelatin complexes strongly enhanced AM production compared with that of naked AM DNA. These results suggest that biodegradable gelatin may serve as a vector for gene transfer. In fact, AM DNA-gelatin complexes induced more potent angiogenic effects in a rabbit model of hind limb ischemia than naked AM DNA, as evidenced by significant increases in histological capillary density, calf blood pressure ratio, laser Doppler flow, and muscle weight ratio and a decrease in necrosis of lower hind limb and thigh muscles. These results suggest that the use of biodegradable gelatin as a nonviral vector augments AM expression and enhances AM-induced angiogenic effects. The angiogenic effects of AM-gelatin complexes were comparable to those of bFGF-gelatin complexes (data not shown). AM DNA-gelatin complexes were distributed mainly in connective tissues. We have recently demonstrated that gelatin-DNA complex is readily phagocytosed by mac-

rophages, monocytes, endothelial progenitor cells, and so on, resulting in gene expression within these phagocytes.[23,24] These findings raise the possibility that AM secreted from these cells acts on muscles in a paracrine fashion. Unlike AM production in the naked AM group, AM overexpression in the AM-gelatin group lasted for longer than 2 weeks. Thus, it is interesting to speculate that delaying gene degradation by gelatin may be responsible for the highly efficient gene transfer.

Currently, a highly efficient and safe gene delivery system is needed for gene therapy in humans. The present study demonstrated that the use of gelatin, which is considered to be less biohazardous than viral vectors, enhanced the angiogenic potential of AM DNA. Thus, gelatin-mediated AM gene transfer may be a new therapeutic strategy for the treatment of severe peripheral vascular diseases. However, the initial success of gelatin-mediated AM gene therapy reported here should be confirmed by long-term experiments, and extensive toxicity studies in animals are needed before clinical trials.

Study Limitation

First, histological capillary density, calf blood pressure ratio, and laser Doppler flow were significantly higher in the AM-gelatin group than in the naked AM group. However, the angiographic score did not significantly differ between the two. This discrepancy raises the possibility that conventional angiography may have insufficient resolution to fully visualize the angiogenic microvessels. Second, human AM level was slightly elevated in the control group. This implies that the anti-human AM antibody used in this radioimmunoassay had some cross-reactivity with endogenous rabbit AM. Nevertheless, human AM level in the muscles was highest in the AM-gelatin group within 2 weeks after gene transfer. These results suggest that AM DNA-gelatin complexes induces potent and long-lasting AM production.

Conclusions

Intramuscular administration of AM DNA induced therapeutic angiogenesis in a rabbit model of chronic hind limb ischemia. Furthermore, the use of biodegradable gelatin as a nonviral vector augmented AM expression and thereby enhanced the therapeutic effects of AM gene transfer. Thus, gelatin-mediated AM gene transfer may be a new therapeutic strategy for the treatment of peripheral vascular diseases.

Acknowledgments

This work was supported by a grant from the Japan Cardiovascular Research Foundation, HLSRG-RAMT-nano-001 and -RHGTEFB-genome-005, RGCD13C-1 from MHLW, grants from NEDO, a Grant-in-Aid for Scientific research from MECSST (13470154 and13877114), and the Promotion of Fundamental Studies in Health Science of the Organization for Pharmaceutical Safety and Research (OPSR) of Japan.

References

1. Kitamura K, Kangawa K, Kawamoto M, et al. Adrenomedullin: a novel hypotensive peptide isolated from human pheochromocytoma. *Biochem Biophys Res Commun.* 1993;192:553–560.
2. Sugo S, Minamino N, Kangawa K, et al. Endothelial cells actively synthesize and secrete adrenomedullin. *Biochem Biophys Res Commun.* 1994;201:1160–1166.
3. Sugo S, Minamino N, Shoji H, et al. Production and secretion of adrenomedullin from vascular smooth muscle cells: augmented production by tumor necrosis factor-alpha. *Biochem Biophys Res Commun.* 1994;203:719–726.
4. Kato J, Kitamura K, Kangawa K, et al. Receptors for adrenomedullin in human vascular endothelial cells. *Eur J Pharmacol.* 1995;289:383–385.
5. Shimekake Y, Nagata K, Ohta S, et al. Adrenomedullin stimulates two signal transduction pathways, cAMP accumulation and Ca^{2+} mobilization, in bovine aortic endothelial cells. *J Biol Chem.* 1995;270:4412–4417.
6. Nagaya N, Satoh T, Nishikimi T, et al. Hemodynamic, renal, and hormonal effects of adrenomedullin infusion in patients with congestive heart failure. *Circulation.* 2000;101:498–503.
7. Nishimatsu H, Suzuki E, Nagata D, et al. Adrenomedullin induces endothelium-dependent vasorelaxation via the phosphatidylinositol 3-kinase/Akt-dependent pathway in rat aorta. *Circ Res.* 2001;89:63–70.
8. Kato H, Shichiri M, Marumo F, et al. Adrenomedullin as an autocrine/paracrine apoptosis survival factor for rat endothelial cells. *Endocrinology.* 1997;138:2615–2620.
9. Sata M, Kakoki M, Nagata D, et al. Adrenomedullin and nitric oxide inhibit human endothelial cell apoptosis via a cyclic GMP-independent mechanism. *Hypertension.* 2000;36:83–88.
10. Kano H, Kohno M, Yasunari K, et al. Adrenomedullin as a novel antiproliferative factor of vascular smooth muscle cells. *J Hypertens.* 1996;14:209–213.
11. Shindo T, Kurihara Y, Nishimatsu H, et al. Vascular abnormalities and elevated blood pressure in mice lacking adrenomedullin gene. *Circulation.* 2001;104:1964–1971.
12. Caron KM, Smithies O. Extreme hydrops fetalis and cardiovascular abnormalities in mice lacking a functional adrenomedullin gene. *Proc Natl Acad Sci U S A.* 2001;98:615–619.
13. Imai Y, Shindo T, Maemura K, et al. Evidence for the physiological and pathological roles of adrenomedullin from genetic engineering in mice. *Ann N Y Acad Sci.* 2001;947:26–34.
14. Shiojima I, Walsh K. Role of Akt signaling in vascular homeostasis and angiogenesis. *Circ Res.* 2002;90:1243–1250.
15. Tabata Y, Hijikata S, Muniruzzaman M, et al. Neovascularization effect of biodegradable gelatin microspheres incorporating basic fibroblast growth factor. *J Biomater Sci Polym Ed.* 1999;10:79–94.
16. Fukunaka Y, Iwanaga K, Morimoto K, et al. Controlled release of plasmid DNA from cationized gelatin hydrogels based on hydrogel degradation. *J Control Release.* 2002;80:333–343.
17. Takeshita S, Zheng LP, Brogi E, et al. Therapeutic angiogenesis: a single intraarterial bolus of vascular endothelial growth factor augments revascularization in a rabbit ischemic hindlimb model. *J Clin Invest.* 1994;93:662–670.
18. Van Belle E, Witzenbichler B, Chen D, et al. Potentiated angiogenic effect of scatter factor/hepatocyte growth factor via induction of vascular endothelial growth factor. *Circulation.* 1998;97:381–390.
19. Ohta H, Tsuji T, Asai S, et al. A simple immunoradiometric assay for measuring the entire molecules of adrenomedullin in human plasma. *Clin Chim Acta.* 1999;287:B131–B143.
20. Nagaya N, Nishikimi T, Yoshihara F, et al. Cardiac adrenomedullin gene expression and peptide accumulation after acute myocardial infarction in rats. *Am J Physiol Regul Integr Comp Physiol.* 2000;278:R1019–R1026.
21. Miyashita K, Itoh H, Sawada N, et al. Adrenomedullin promotes proliferation and migration of cultured endothelial cells. *Hypertens Res.* 2003;26:S93–S98.
22. Jiang BH, Zheng JZ, Aoki M, et al. Phosphatidylinositol 3-kinase signaling mediates angiogenesis and expression of vascular endothelial growth factor in endothelial cells. *Proc Natl Acad Sci U S A.* 2000;97:1749–1753.
23. Tabata Y, Ikada Y. Macrophage activation through phagocytosis of muramyl dipeptide encapsulated in gelatin microspheres. *J Pharm Pharmacol.* 1987;39:698–704.
24. Nagaya N, Kangawa K, Kanda M, et al. Hybrid cell-gene therapy for pulmonary hypertension based on phagocytosing action of endothelial progenitor cells. *Circulation.* 2003;108:889–895.

J|A|C|S
COMMUNICATIONS

Published on Web 02/11/2005

PEGylated Polyplex Micelles from Triblock Catiomers with Spatially Ordered Layering of Condensed pDNA and Buffering Units for Enhanced Intracellular Gene Delivery

Shigeto Fukushima,[†,§] Kanjiro Miyata,[†,#] Nobuhiro Nishiyama,*[,‡] Naoki Kanayama,[†,#] Yuichi Yamasaki,[†,#] and Kazunori Kataoka*[,†,‡,#]

Department of Materials Science and Engineering, Graduate School of Engineering, The University of Tokyo, 7-3-1 Hongo, Bunkyo-ku, Tokyo 113-8656, Japan, Center for Disease Biology and Integrative Medicine, Graduate School of Medicine, The University of Tokyo, Tokyo 113-0033, Japan, Nippon Kayaku Co., Ltd., and CREST, Japan Science and Technology Agency, Japan

Received September 29, 2004; E-mail: nishiyama@bmw.t.u-tokyo.ac.jp; kataoka@bmw.t.u-tokyo.ac.jp

Successful in vivo gene therapy relies on the development of efficient gene vectors. Especially, the synthetic vectors based on cationic polymers have been attracting much attention because of their safety for clinical application and the variety of their chemical design. Nevertheless, the rational design of synthetic vectors remains to be established. Many previous studies have described that polyplexes formed from polycations with a comparatively low pK_a values, such as polyethylenimine (PEI), show a high transfection activity,[1] which has been explained by the proton sponge effect.[2] However, such polycations have a weak affinity to DNA, resulting in the formation of polyplexes that are easily dissociated under physiological conditions. Also, the buffer capacity of polycations may be hampered by their facilitated protonation due to the zipper effect or the neighboring group effect during the complexation process with DNA.[3] These problems could be modulated by the addition of excess polycations (i.e., increasing the N/P ratios[4]) to form polyplexes with a cationically deviated composition. However, it was recently demonstrated that free polycations in such polyplexes substantially contribute to efficient transfection but also mediate toxic effects. Hence, polyplex systems useful for in vivo gene delivery are required to achieve efficient transfection under the condition without free polycations.[5] Also, the gene delivery systems need to be equipped with high stability and biocompatibility. Here, A−B−C type triblock copolymers consisting of three distinctive functional segments were newly designed for constructing gene delivery systems which might not require free polycations to achieve enhanced gene expression but might provide a high stability and biocompatibility. In the present design of triblock copolymers, poly(ethylene glycol) (PEG) was used as the biocompatible A-segment, poly[(3-morpholinopropyl) aspartamide] (PMPA) was used as the low-pK_a B-segment with a buffering capacity, and poly(L-lysine) (PLL) was used as the high-pK_a C-segment to condense the DNA (Figure 1).

The triblock copolymer, PEG−PMPA−PLL, was synthesized by the successive ring-opening polymerization of the *N*-carboxyanhydrides (NCAs) of β-benzyl-L-aspartate (BLA) and ϵ-(benzyloxycarbonyl)-L-lysine (Lys(Z)), initiated by the $-NH_2$ group of α-methoxy-ω-amino PEG (MW 12 000), followed by the aminolysis of the benzyl ester of PBLA using 4-(3-aminopropyl)morpholine and the deprotection of the Z groups of PLL(Z).[6] The triblock copolymer was confirmed to have a narrow molecular weight distribution (M_w/M_n = 1.18), and the number of repeating units of PMPA and PLL was calculated to be 36 and 50, respectively, from the ^{1}H NMR. Diblock copolymers, PEG−PLL with 48 PLL units and PEG−PMPA with 39 PMPA units, were used as comparative samples in this study. The formation of polyplex micelles from these block catiomers was confirmed by a gel retardation assay (Figure S4, Supporting Information).[6] Also, the interaction between the di- or triblock copolymers and plasmid DNA (pDNA) was evaluated by an ethidium bromide (EtBr) exclusion assay (Figure 2a). In the case of PEG−PLL (pK_a 9.4), the fluorescence intensity was decreased to 20% of that of the naked pDNA at the N/P ratio of 2. In contrast, the system of PEG−PMPA, having a cationic segment with a lower pK_a value (pK_a 6.2), maintained relatively high fluorescence (>90%) over a wide range of N/P ratios, suggesting that PEG−PMPA lacks the capacity to condense pDNA to a level detectable by this assay. On the other hand, PEG−PMPA−PLL exhibited an 80% decrease in fluorescence at the N/P ratio of 3. Interestingly, the fluorescence profile of PEG−PMPA−

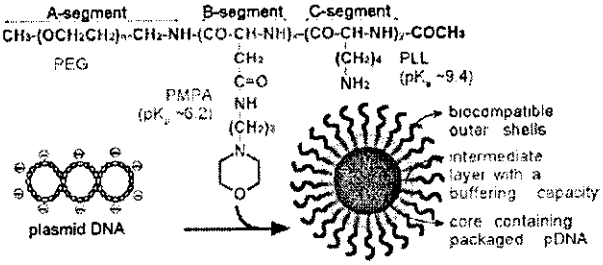

Figure 1. Chemical structure of PEG−PMPA−PLL triblock copolymers and schematic illustration of the hypothesized three-layered polyplex micelles with spatially regulated structure.

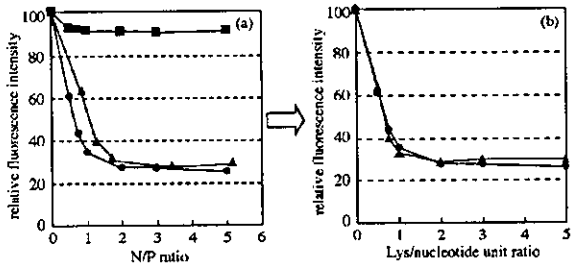

Figure 2. Interaction of PEG−PLL (circle), PEG−PMPA (square), and PEG−PMPA−PLL (triangle) copolymers with pDNA in 10 mM PBS (pH 7.4) + 150 mM NaCl, evaluated by dye exclusion assay. (a) In this figure, the *X*-axis represents the N/P ratio, where N stands for the total of MPA and Lys units. (b) In this figure, the *X* axis represents the Lys/nucleotide unit ratio.

† Graduate School of Engineering, The University of Tokyo.
‡ Graduate School of Medicine, The University of Tokyo.
§ Nippon Kayaku Co., Ltd.
# CREST, Japan Science and Technology Agency.

10.1021/ja0440506 CCC: $30.25

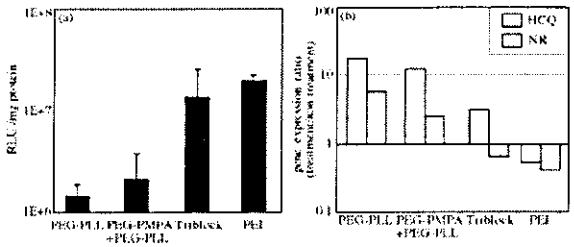

Figure 3. In vitro transfection of luciferase gene to HeLa cells by polyplex micelles from di- or triblock copolymers. HeLa cells were incubated with each micelle in the medium containing 10% serum for 24 h, followed by an additional 24 h incubation without the micelles. (a) The polyplex micelles were prepared at a Lys/nucleotide ratio of 2, and the PEI/pDNA was prepared at the corresponding N/P ratio to the PEG−PMPA−PLL/pDNA. (b) The effects of HCQ and NR on the TE of the polyplexes were evaluated. The PEI polyplex was prepared at the N/P ratio of 10.

PLL/pDNA was almost identical to that of PEG−PLL/pDNA when the N/P ratio was converted to the Lys/nucleotide unit ratio (Figure 2b). Presumably, in the complex of PEG−PMPA−PLL/pDNA, the PLL segment may predominantly contribute to the pDNA condensation. This assumption was confirmed by ^{1}H NMR measurement of PEG−PMPA−PLL/pDNA [Lys/nucleotide ratio = 2 (N/P ratio = 3.4)] in deutereted phosphate-buffered saline (pD 7.4, 150 mM NaCl), in which the chemical shifts assigned to the PLL segment completely disappeared but those assigned to the PMPA segments remained in the spectrum (Figure S6, Supporting Information).[6] This result is consistent with the hypothesis that the PEG−PMPA−PLL/pDNA may form three-layered polyplexes as illustrated in Figure 1. Also, the complete disappearance of PLL peaks from the NMR spectrum suggests that PEG−PMPA−PLL in free form may be minimal in the solution. The size and ζ-potential of the PEG−PMPA−PLL complexes at the Lys/nucleotide ratio of 2 were determined to be 88.7 nm and 7.3 mV, respectively, comparable to those obtained from the PEG−PLL complexes at the N/P ratio of 2 (91.7 nm and 2.1 mV, respectively). The particle size of approximately 100 nm is consistent with the condensed structure of pDNA, and the low absolute value of the ζ-potential suggests the formation of the PEG palisade surrounding the polyplex core.

In vitro transfection efficiency (TE) of the PEG−PMPA−PLL/pDNA at the Lys/nucleotide ratio of 2 was evaluated against HeLa cells. Notably, PEG−PMPA−PLL/pDNA revealed 1 order of magnitude higher TE than PEG-PLL/pDNA (Figure 3a), which was comparable to that of the PEI/pDNA at the corresponding N/P ratio, without showing appreciable cytotoxicity (Figure S9, Supporting Information).[6] On the other hand, the TE of the system composed of (PEG−PMPA + PEG−PLL)/pDNA, where the contents and the repeating units of the PMPA and PLL segments were nearly equal to PEG−PMPA−PLL, was almost the same as that of PEG−PLL. Also, the polyplexes of PEG−PMPA showed no transfection activity over a wide range of N/P ratios (data not shown). These results strongly indicate the importance of aligning in tandem two types of polycations with different pK_a values in a single polymer strand. To study the mechanism of the transfection, the effects of hydroxychloroquine (HCQ) and nigericin (NR) on transfection behavior were investigated. HCQ is known to increase the TE of the polyplexes lacking a buffering capacity, whereas NR could decrease the TE of the polyplexes showing the proton sponge effect.[7] The PEG−PMPA−PLL/pDNA showed less effect of HCQ on enhancing the gene expression compared with the PEG−PLL/pDNA, while it showed an appreciable decrease in the TE in the presence of NR (Figure 3b). Similar trends were also confirmed for 293T cells (Figure S8, Supporting Information). These biological results are consistent with the hypothesis that the enhanced TE of the PEG−PMPA−PLL/pDNA may be attributed to the proton sponge effect. Thus, the buffering capacity of PMPA segment appears to be maintained in the PEG−PMPA−PLL/pDNA under the condition with low Lys/nucleotide ratio. The preferential contribution of the PLL segment to the DNA condensation may ensure the presence of the uncomplexed PMPA segment, even at a comparatively low N/P ratio, to work as a buffering unit.[6]

Nonviral gene vectors used in vivo must have a high stability to be tolerated under harsh conditions in the body. In our previous studies, polyplexes based on PEG−PLL showed a high serum tolerability[8] and prolonged blood circulation.[9] Although the PLL segments form stable polyplexes with pDNA, the transfection activity might be inefficient due to the lack of a proton buffering capacity. In contrast, polycations with a lower pK_a have a buffering capacity for the enhanced transfection but demand a high N/P ratio to achieve a high efficacy. Polyplexes formed at a high N/P ratio may not be useful for in vivo transfection due to stability and toxicity concerns.[5] The result reported here led to the novel design of nonviral gene vectors, overcoming the problems of conventional systems based on the proton sponge concept, using the A−B−C type triblock copolymers, PEG−PMPA−PLL (Figure 1). The results are consistent with the hypothesis that PEG−PMPA−PLL might form three-layered polyplex micelles consisting of a core of pDNA/PLL polyion complexes, an intermediate layer of PMPA segments with a buffer capacity, and an outer shell of biocompatible PEG segments. The PEG−PMPA−PLL polyplexes showed a significantly enhanced transfection activity through the buffering capacity of the PMPA segment, while efficiently compacting pDNA by the PLL segment. Importantly, this increased transfection was achieved under the condition where free or loosely associated polycations are assumed to be minimal, facilitating the future utility of this polyplex micelle for in vivo gene delivery.

Acknowledgment. This work was supported by the Core Research for Evolutional Science and Technology (CREST) from the Japan Science and Technology Agency (JST).

Supporting Information Available: Synthetic method and characterization of triblock copolymers as well as additional data on the physicochemical and biological properties of the PEG−PMPA−PLL/pDNA. This material is available free of charge via the Internet at http://pubs.acs.org.

References

(1) (a) Boussif, O.; Lezoualc'h, F.; Zanta, M. A.; Mergny, M. D.; Scherman, D.; Demeneix, B.; Behr, J.-P. *Proc. Natl. Acad. U.S.A.* **1995**, *92*, 7297−7301. (b) Tang, M. X.; Szoka, F. C. *Gene Ther.* **1997**, *4*, 823−832. (c) Midoux, P.; Monsigny, M. *Bioconjugate Chem.* **1999**, *10*, 406−411. (d) Cherng, J.-Y.; Wetering, P.; Talsma, H.; Crommelin, D. J. A.; Hennink, W. E. *Pharm. Res.* **1996**, *13*, 1038−1042.
(2) Behr, J.-P. *Chemia* **1997**, *51*, 34−36.
(3) Kabanov, A. V.; Bronich, T. K.; Kabanov, V. A.; Yu, K.; Eisenberg, A. *Macromolecules* **1996**, *29*, 6797−6802.
(4) The ratio of the cationic moiety in polycations to the phosphate in DNA.
(5) Boeckle, S.; Gersdorff, K.; Piepen, S.; Culmsee, C.; Wagner, E.; Ogris, M. *J. Gene Med.* **2004**, *6*, 1102−1111.
(6) See Supporting Information.
(7) Lim, Y.-B.; Kim, S.-M.; Suh, H.; Park, J.-S. *Bioconjugate Chem.* **2002**, *13*, 952−957.
(8) (a) Itaka, K.; Harada, A.; Nakamura, K.; Kawaguchi, H.; Kataoka, K. *Biomacromolecules* **2002**, *3*, 841−845. (b) Itaka, K.; Yamauchi, K.; Harada, A.; Nakamura, K.; Kawaguchi, H.; Kataoka, K. *Biomaterials* **2003**, *24*, 4495−4506.
(9) Harada-Shiba, M.; Yamauchi, K.; Harada, A.; Takamisawa, I.; Shimokado, K.; Kataoka, K. *Gene Ther.* **2002**, *9*, 407−414.

JA0440506

J|A|C|S
COMMUNICATIONS

Published on Web 01/22/2005

Lactosylated Poly(ethylene glycol)-siRNA Conjugate through Acid-Labile β-Thiopropionate Linkage to Construct pH-Sensitive Polyion Complex Micelles Achieving Enhanced Gene Silencing in Hepatoma Cells

Motoi Oishi,[†,⊥] Yukio Nagasaki,*[,†,⊥] Keiji Itaka,[‡] Nobuhiro Nishiyama,[§] and Kazunori Kataoka*[,§]

Department of Materials Science and Technology, Tokyo University of Science, 2641 Yamazaki, Noda, Chiba 278-8510, Japan, Department of Orthopaedic Surgery, Faculty of Medicine, The University of Tokyo, 7-3-1 Hongo, Bunkyo-ku, Tokyo 113-8655, Japan, and Department of Materials Science and Engineering, Graduate School of Engineering, The University of Tokyo, 7-3-1 Hongo, Bunkyo-ku, Tokyo 113-8656, Japan

Received August 20, 2004; E-mail: kataoka@bmw.t.u-tokyo.ac.jp; nagasaki@nagalabo.jp

Nucleic acid medicines such as antisense DNAs[1] and small, interfering RNAs (siRNAs)[2] have attracted much attention as a new class of therapeutic agents. In particular, siRNAs are recently recognized as the most powerful tools for sequence-specific gene silencing via naturally occurring RNA interference (RNAi) process.[3] Nevertheless, the therapeutic value of siRNAs under in vivo conditions is still controversial due to their low stability against enzymatic degradation, low permeability across cell membrane, and preferential liver and renal clearance.[4] A major key to the therapeutic success of siRNA is believed to be the development of carrier systems achieving the modulated disposition in the body through the intravenous route as well as the smooth transport of intact siRNA into the interior of the target cell. Worth noticing in this regard is a new class of nanometric-scaled carriers (nanocarriers) of oligonucleotides formulated through the self-assembly of PEG-based block ionomers (polyion complex (PIC) micelles).[5] Both combinations of PEG-*block*-polycation/oligonucleotide and PEG-*block*-oligonucleotide (or PEG-oligonucleotide conjugate)/polycation are feasible for PIC micelle formulation with a segregated PIC core surrounded by a palisade of flexible and hydrophilic PEG layers to increase biocompatibility and enzymatic tolerability. Ligands may be installed on the periphery of the PEG palisade of the PIC micelles to increase the uptake into the target cells through a receptor-mediated endocytotic pathway.[6] A unique finding, which we would like to communicate here, is the remarkably enhanced RNAi in cultured hepatoma cells through the assembly of siRNA into smart lactosylated-PIC micelles with pH-sensitive dissolution properties, thus achieving an appreciable silencing of the target gene at an extremely low siRNA concentration.

Our strategy of formulating pH-sensitive and targetable PIC micelles of siRNA is based on the novel conjugation of siRNA with lactosylated PEG through acid-labile linkage of β-thiopropionate (Lac-PEG-siRNA; Figure 1), followed by the complexation with poly(L-lysine). Note that β-thiopropionate linkage (3-sulfanylpropionyl linkage)[7] is readily cleaved at the pH corresponding to that of the intracellular endosomal compartment (pH = 5.5).[5a] Michael addition of the 5′-thiol-modified sense RNA (firefly luciferase, pGL3-control sense sequence) toward the ω-acrylate group of the α-lactosyl-ω-acryl-PEG gave a conjugate of Lac-PEG with single-stranded RNA (Lac-PEG-ssRNA), which revealed a retarded migration in gel electrophoretic assay (Figure 2, lane 3) compared to free-sense RNA (Figure 2, lane 1) in line with

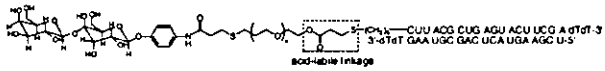

Figure 1. Chemical structure of the Lac-PEG-siRNA conjugate.

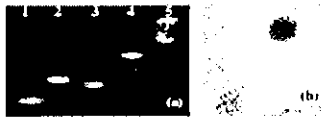

Figure 2. (a) Polyacrylamide gel retardation assay: lane 1, sense RNA; lane 2, siRNA; lane 3, Lac-PEG-ssRNA; lane 4, Lac-PEG-siRNA; and lane 5, PIC micelle. (b) Transmission electron micrograph of the disulfide cross-linked PIC micelle.

PEGylation. Then, the Lac-PEG-ssRNA was annealed with antisense RNA to undergo hybridization, preparing the Lac-PEG conjugate with siRNA (Lac-PEG-siRNA). The Lac-PEG-siRNA thus prepared gave a single band in gel electrophoresis (lane 4) and had further retarded migration compared to Lac-PEG-ssRNA (lane 3) and free siRNA (lane 2). All of these results are consistent with the successful preparation of the Lac-PEG-siRNA with negligible contamination with unreacted and intermediate compounds.

The PIC micelles from the Lac-PEG-siRNA conjugate and PLL (degree of polymerization = 40) were then prepared at the charge ratio of 1 (N/P = 1), where no free Lac-PEG-siRNA conjugate and almost complete retardation were observed in a polyacrylamide gel electrophoresis (Figure 2a, lane 5), suggesting that polyion complexation between the siRNA segment and the PLL quantitatively took place. The PIC micelle with disulfide cross-linked core was also prepared by using thiolated PLL (see Supporting Information) tolerable for the transmission electron microscopy (TEM) observation. As seen in Figure 2b, the disulfide cross-linked PIC micelles have spherical shapes with an average size (n = 36) of 117 ± 26 nm, consistent with the formation of multimolecular micellization of the Lac-PEG-siRNA with PLL.

The dual luciferase reporter assay was done in HuH-7 cells (human hepatoma cells) possessing asialoglycoprotein (ASGP) receptors, which recognize compounds bearing terminal galactose moieties,[8] to evaluate the gene silencing ability of the conjugate and the PIC micelle system (Figure 3). Both the Lac-PEG-siRNA conjugate and the PIC micelle (N/P = 1) revealed RNAi activities with a dose-dependent manner even in the presence of 10% FBS, and in particular, the PIC micelles achieved far more effective RNAi activity than the Lac-PEG-siRNA conjugate alone, viz., 50% inhibitory concentration (IC_{50}) was found to be 1.3 nM and 91.4 nM for the PIC micelle and Lac-PEG-siRNA conjugate, respec-

† Tokyo University of Science.
‡ Faculty of Medicine, The University of Tokyo.
§ Graduate School of Engineering, The University of Tokyo.
⊥ Current address: Tsukuba Research Center for Interdisciplinary Materials Science (TIMS), University of Tsukuba, 1-1-1 Tennoudai, Tsukuba, Ibaragi 305-8573, Japan.

10.1021/ja044941d CCC: $30.25

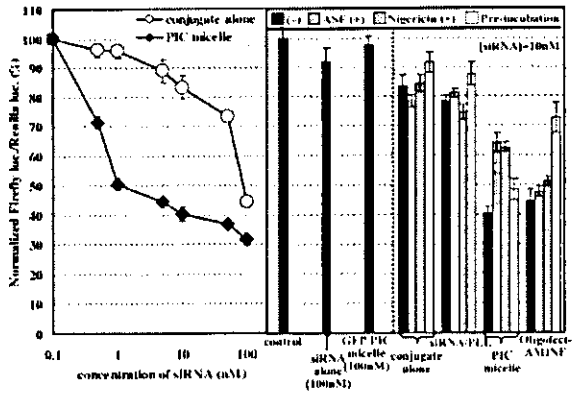

Figure 3. RNAi activities against the firefly luciferase gene generated in cultured HuH-7 cells. Normalized ratios between the firefly luciferase activity (firefly luc.) and the renilla luciferase activity (renilla luc.) are shown on the ordinate. The indicated concentrations of siRNA were the final concentrations in the total transfection volume (250 μL). The plotted data are averages of triplicate experiments ± SD. P^* < 0.05 (vs Lac-PEG-siRNA conjugate).

tively. This almost 100 times increase in RNAi activity by PIC micelle is remarkable.

On the other hand, no RNAi activity was observed for free siRNA even at 100 nM of siRNA concentration. The lack of RNAi activity for free siRNA may be ascribed to the low tolerability against enzymatic attack[5a] and/or the restricted uptake into the cellular interior due to the elcetrostatic repulsion with the negatively charged plasma membranes. Note that the PIC micelle including a GFP sequence induced no RNAi, strongly suggesting that an inhibition of firefly luciferase expression observed here indeed occurred through the sequence-specific RNAi effect. In addition, siRNA/PLL (polyplex) showed significantly lower RNAi activity compared to the PIC micelle probably owing to the aggregation at charge-neutralized conditions (N/P = 1) and nonspecific interaction with serum proteins. Although the RNAi activity for the PIC micelle at 10 nM of conjugate concentrations was the same level compared to the commercially available oligofectAMINE (cationic liposome), the RNAi activity for the oligofectAMINE after preincubation with 50% serum for 30 min was significantly reduced (56 → 27% inhibition, P < 0.05) due to the nonspecifically interacting nature of the cationic carriers with negatively charged serum proteins. In sharp contrast, the PIC micelle still retained the RNAi activity even after preincubation for 30 min with 50% serum due to the segregation of the siRNA into the PEG environment.[9] To confirm the cellular uptake pathway, asialofetuin (ASF) as the inhibitor for the ASGP receptor-mediated endocytosis[10] was added to the culture medium (4 mg/mL). As a consequence, RNAi activities were reduced significantly for the PIC micelles (60 → 36% inhibition, P < 0.05), whereas there was negligible effect of ASF on RNAi activities for Lac-PEG-siRNA conjugate, siRNA/PLL, and oligofectAMINE in HuH-7 cells (Figure 3). Note that no effect of ASF was observed for ASGP receptor-negative NIH 3T3 cells (mouse fibroblast) even for the PIC micelles (see Supporting Information). Obviously, these results indicate that the lactose moieties clustering on the surface of PIC micelle appreciably facilitates ASGP receptor-mediated endocytosis to direct a remarkable RNAi efficacy. Then, nigericin as the inhibitor for the endosomal acidification[11] was added to the culture medium (5 μM) to confirm that the acid-labile linkage in the conjugate contributes RNAi activity. Consequently, the RNAi activity was significantly reduced for the PIC micelle (60 → 37% inhibition, P < 0.05), whereas no effect was observed for the Lac-PEG-siRNA conjugate, siRNA/PLL, and the oligofectAMINE. This result suggests that after the endocytotic internalization the cleavage of the acid-labile linkage of the micelles occurred in the manner synchronized with the pH decrease in the endosomal compartment, releasing hundreds of free PEG strands to increase the colloidal osmotic pressure. This may induce the swelling and disruption of the endosome,[12] facilitating the transport of free siRNA into the cytoplasm. Several important factors are likely to be synergistically involved in the pronounced RNAi activity of the PIC micelles, such as the improvement of the stability against enzymatic degradation, minimal interaction with serum proteins, enhancement of the cellular uptake through the ASGP receptor-mediated endocytosis, and the effective transport of free siRNA from endosome into cytoplasm. It should be noted that the PIC micelles entrapping the Lac-PEG-siRNA conjugate reported here showed about 5800 times higher gene-silencing effect compared to that entrapping the Lac-PEG-antisense DNA conjugate targeting the same gene sequence (IC_{50} = 7.6 μM).[13]

In conclusion, the pH-responsive and targetable PIC micelle composed of PLL and Lac-PEG-siRNA conjugate bearing an acid-labile linkage exhibited significant gene silencing for firefly luciferase expression in HuH-7 cells. Therefore, this approach of PIC micellization of PEG-siRNA conjugate with an appropriate polycation has promise as a targetable siRNA delivery system used in a practical context. Further study on gene silencing against endogenous genes as well as in vivo performance is now in progress in our laboratories.

Acknowledgment. This work was supported by the Core Research for Evolutional Science and Technology (CREST) from the Japan Science and Technology Agency [JST]. We appreciate Mr. Teisaku Nakamura for taking the TEM image.

Supporting Information Available: Experimental details, materials, and the dual luciferase reporter assay. This material is available free of charge via the Internet at http://pubs.acs.org.

References

(1) (a) Crooke, S. T. *Biotechnol. Genet. Eng. Rev.* **1998**, *15*, 121. (b) Cook, P. D. *Handb. Exp. Pharmacol.* **1998**, *131*, 51.
(2) Elbashir, S. M.; Harborth, J.; Lendeckel, W.; Yalcin, A.; Weber, K.; Tuschl, T. *Nature* **2001**, *411*, 494.
(3) Taira, H. K. *Nucleic Acid Res.* **2003**, *31*, 700. (c) Miyagishi, M.; Taira, K. *Nat. Biotechnol.* **2002**, *20*, 497.
(4) Braasch, D.; Paroo, Z.; Constantiescu, A.; Ren, G.; Öz, O. K.; Mason, R. P.; Corey, D. R. *Bioorg. Med. Chem. Lett.* **2004**, *14*, 1139.
(5) For selected examples, see: (a) Oishi, M.; Sasaki, S.; Nagasaki, Y.; Kataoka, K. *Biomacromolecules* **2003**, *4*, 1426. (b) Jeong, J. H.; Kim, S. W.; Park, T. G. *Bioconjugate Chem.* **2003**, *14*, 473. (c) Vinogradov, S. V.; Bronich, T. K.; Kabanov, A. V. *Bioconjugate Chem.* **1998**, *9*, 805. (d) Kataoka, K.; Togawa, H.; Harada, A.; Yasugi, K.; Matsumoto, T.; Katayose, S. *Macromolecules* **1996**, *29*, 8556. (e) Harada, A.; Kataoka, K. *Macromolecules* **1995**, *28*, 5294.
(6) Wakebayashi, D.; Nishiyama, N.; Yamasaki, Y.; Itaka, K.; Kanayama, N.; Harada, A.; Nagasaki, Y.; Kataoka, K. *J. Controlled Release* **2004**, *95*, 653.
(7) Schoenmakers, R. G.; van de Wetering, P.; Elbert, D. L.; Hubbell, J. A. *J. Controlled Release* **2004**, *95*, 291.
(8) Wu, C. H.; Wu, G. Y. *Adv. Drug Delivery Rev.* **1998**, *29*, 243.
(9) Itaka, K.; Kanayama, N.; Nishiyama, N.; Jang, W.-D.; Yamasaki, Y.; Nakamura, K.; Kawaguchi, H.; Kataoka, K. *J. Am. Chem. Soc.* **2004**, *126*, 13612.
(10) Zanta, M. A.; Boussif, O.; Adib, A.; Behr, J. P. *Bioconjugate Chem.* **1997**, *8*, 839.
(11) Uherek, C.; Fominaya, J.; Wels, W. *J. Biol. Chem.* **1998**, *273*, 8835.
(12) Goh, S. L.; Murthy, N.; Xu, M.; Fréchet, J. M. J. *Bioconjugate Chem.* **2004**, *15*, 467.
(13) Oishi, M.; Nagatsugi, F.; Sasaki, S.; Nagasaki, Y.; Kataoka, K. *ChemBioChem.* In press.

JA044941D

were used as the substrates. PFMA was prepared according to the procedure previously reported by Arai et al. [15].

Chemical Modification of the Glass Surface: The surface treatment of glass substrates was performed according to previously described procedures [16]. The individual steps are summarized briefly in the following. The substrates were ultrasonically cleaned in a washing agent (Extran MA 01, Merck Ltd.) in order to eliminate organic contamination from the surface. They were then rinsed with distilled water and dried. Next, the substrate was placed in a reaction vessel, to which was added 1 % (v/v) GPS and 0.2 % (v/v) triethylamine in anhydrous toluene. The mixture was stirred and kept at 70 °C for 4 h before washing with toluene and acetone. The substrate was then dried in a vacuum overnight at 50 °C. The obtained surface, bearing terminal epoxy groups, was hydrolyzed by immersing the substrate in a 100 mM NaCl solution adjusted to pH 4 with 10 mM HCl, heated to 70 °C for 30 min, then rinsed with distilled water and dried in a vacuum. Finally, the surface bearing terminal hydroxyl groups was immersed in a solution of 2-furoic chloride (26 mg, 0.2 mmol) in acetone (20 mL) and pyridine (23 mg, 0.3 mmol); this solution was stirred at room temperature for 24 h. It was then rinsed with distilled water and acetone and dried in a vacuum. The substrates with furan-functionalized surfaces were stored in a N_2 atmosphere.

Characterization: The molecular weight of obtained polymer, PFMA, was estimated by gel permeation chromatography with two Tosho columns (G4000HXL and G3000HXL) using tetrahydrofuran (THF) as the eluent at 40 °C after calibration with standard polystyrene. UV-visible spectroscopy (UV-3100s, Shimadzu Co.) was used to confirm the surface modification by the furan functional groups. AFM images of the sample surfaces were taken with a Nanoscope III (Digital Instruments) in a tapping mode operated under ambient conditions. The cantilever used was a commercially available etched silicon probe (TESP, Digital Instruments, Inc.) 125 μm long and with resonant frequencies of 294–356 kHz. Electrical resistivity measurements were carried out by means of a four-probe technique, using a high-performance low resistivity meter (MPC-T600, Dia Instruments Co., Ltd.).

Received: September 16, 2003
Final version: December 1, 2003

[1] M. Fuhrer, J. Nygård, L. Shih, M. Forero, Y. Yoon, M. S. C. Mazzoni, H. J. Choi, J. Ihm, S. G. Louie, A. Zettl, P. L. McEuen, *Science* **2000**, *288*, 494.
[2] N. A. Melosh, A. Boukai, F. Diana, B. Gerardot, A. Badolato, P. M. Petroff, J. R. Heath, *Science* **2003**, *300*, 112.
[3] B. Messer, J. H. Song, P. Yang, *J. Am. Chem. Soc.* **2000**, *122*, 10232.
[4] T. Rueches, K. Kim, E. Joselevich, G. Y. Tseng, C. Cheung, C. M. Lieber, *Science* **2000**, *289*, 94.
[5] a) S. Liu, R. Maoz, G. Schmid, J. Sagiv, *Nano Lett.* **2002**, *2*, 1055. b) R. Maoz, E. Frydman, S. R. Cohen, J. Sagiv, *Adv. Mater.* **2000**, *12*, 424. c) R. Maoz, E. Frydman, S. R. Cohen, J. Sagiv, *Adv. Mater.* **2000**, *12*, 725.
[6] a) Y. Huang, X. Duan, Q. Wei, C. M. Lieber, *Science* **2001**, *291*, 630. b) H. O. Jacobs, S. A. Campbell, M. G. Steward, *Adv. Mater.* **2002**, *14*, 1553. c) M. S. Sander, A. L. Prieto, R. Gronsky, T. Sands, A. M. Stacy, *Adv. Mater.* **2002**, *14*, 665. d) N. Saito, H. Haneda, T. Sekiguchi, N. Ohashi, I. Sakaguchi, K. Koumoto, *Adv. Mater.* **2002**, *14*, 418.
[7] P. Buffat, J. P. Borel, *Phys. Rev. A* **1976**, *13*, 2287.
[8] G. Schmid, *Chem. Rev.* **1972**, *92*, 1709.
[9] The surface density of furan-functionalized silane on the substrate surface was confirmed, using UV-vis spectroscopy, as ~26 Å²/silane. This is almost the same as the calculated surface density for the occupation area of the furan moiety (~25 Å²), which means that the functional moieties were introduced almost in a close packing on the surface.
[10] T. Oku, K. Suganuma, *Chem. Commun.* **1999**, 2355.
[11] T. Oku, K. Suganuma, *Microelectron. Eng.* **2000**, *51*, 51.
[12] S. J. Zhao, S. Q. Wang, D. Y. Cheng, H. Q. Ye, *J. Phys. Chem. B* **2001**, *105*, 12857.
[13] R. R. Couchman, *Philos. Mag. A* **1979**, *40*, 637.
[14] R. S. Berry, *Sci. Am.* **1990**, *August*, 263.
[15] H. Arai, Y. Tajima, K. Takeuchi, *Jpn. J. Appl. Phys.* **2001**, *40*, 6623.
[16] G. Jogikalmath, J. K. Stuart, A. Pungor, V. Hlady, *Colloids Surf. A* **1999**, *146*, 337.

Size-Controlled Formation of a Calcium Phosphate-Based Organic–Inorganic Hybrid Vector for Gene Delivery Using Poly(ethylene glycol)-*block*-poly(aspartic acid)**

By *Yoshinori Kakizawa*, *Kanjiro Miyata*, *Sanae Furukawa*, and *Kazunori Kataoka**

Recently, the growing interest in non-viral vector systems for in vivo gene therapy has become a strong incentive to develop a variety of advanced materials for DNA delivery with high efficiency and minimal toxicity.[1–7] Calcium phosphate (CaP)/DNA coprecipitate is one of these materials, and has been widely used for the transfection of plasmid DNA (pDNA)[8,9] and oligonucleotides (ODN)[10] into mammalian and plant cells. Nevertheless, a serious drawback of this system is that, after the initial mixing of the calcium and phosphate solutions, the growth of the CaP crystal is uncontrollably rapid, resulting in large precipitates and a steep drop in the transfection efficacy within a short period of time.[11] This uncontrollable crystal growth also causes handling and reproducibility problems. We wish to now describe a new methodology to control the calcium phosphate growth using a block copolymer with a polycarboxylate segment: poly(ethylene glycol)-*block*-poly(aspartic acid) (PEG-PAA).[12] Using PEG-PAA allows modulation of the crystal size to form a novel nanovector for pDNA with optimized transfection efficiency. The underlying concept is to prevent crystal growth through the absorption of the PAA segment of PEG-PAA on the crystal surface. This leads to the formation of core–shell particles

[*] Prof. K. Kataoka, K. Miyata
Department of Materials Science and Engineering
Graduate School of Engineering, The University of Tokyo
7-3-1 Hongo, Bunkyo-ku, Tokyo 113-8656 (Japan)
E-mail: kataoka@bmw.t.u-tokyo.ac.jp
Prof. K. Kataoka, Dr. Y. Kakizawa, S. Furukawa
Biomaterials Center, National Institute for Materials Science
1-1 Namiki, Tsukuba, Ibaraki 305-0044 (Japan)

[**] This work was supported by the Special Coordination Funds for Promoting Science and Technology from the Ministry of Education, Science, Sports and Culture, Japan (MEXT), and Core Research for Evolutional Science and Technology (CREST), the Japan Science and Technology Corporation (JST).

 DOI: 10.1002/adma.200305782

with a hybrid core of the CaP crystal and pDNA surrounded by a PEG shell. Particle properties such as size, pDNA content, and nuclease resistance of the complexed pDNA were comprehensively studied in relation to the concentration of PEG-PAA.

The effect of PEG-PAA concentration on hybrid particle formation was first investigated by a turbidity measurement based on the standard protocol of CaP/DNA coprecipitation, in which the calcium and phosphate concentrations were kept constant.[11] Figure 1 shows the time course of the change in transmittance at 350 nm after the phosphate/PEG-PAA solution was added to the calcium/DNA solution at 25 °C. In the

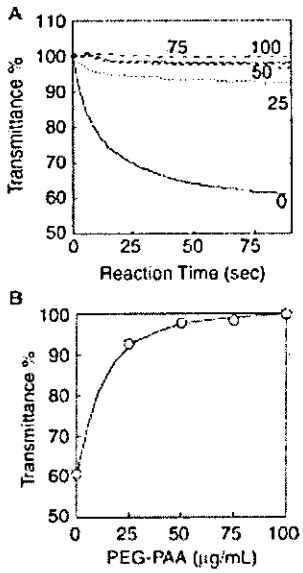

Figure 1. Effect of PEG-PAA on the growth of the calcium phosphate crystals. A) Change in the transmittance of the solutions with reaction time. Numbers denote the PEG-PAA concentration in micrograms per milliliter. B) Transmittance 90 s after mixing the solutions containing various concentrations of PEG-PAA.

absence of the polymer (solid line), the solution's transmittance decreased steeply in the early stage of the reaction, dropping to 60 % of the initial value within 90 s, reflecting the rapid formation of large aggregates of calcium phosphate crystals. Conversely, the increased addition of PEG-PAA from 25 to 100 $\mu g\,mL^{-1}$ progressively prevented solution turbidity and 97 % of the initial transmittance value was exceeded above a concentration of 50 $\mu g\,mL^{-1}$ of the block copolymer. These results clearly show the inhibitory effect of PEG-PAA on the growth and/or secondary aggregation of the CaP/PAA particles.

The size of the hybrid particles was then evaluated using optical microscopy and dynamic light scattering (DLS) measurements. As expected, the size of the ternary hybrid particles of CaP/pDNA/PEG-PAA was found to be inversely correlated to the PEG-PAA concentration, which is consistent with the results of the turbidity measurement. Precipitates of several hundred micrometers to a few millimeters were observed by optical microscopy for the samples prepared in the concentration range of 0–25 $\mu g\,mL^{-1}$ of PEG-PAA. On the other hand, in PEG-PAA concentrations higher than 50 $\mu g\,mL^{-1}$, there is a drastic reduction in the particle diameter. Indeed, the DLS measurements revealed that the hydrodynamic diameters of the particles are progressively reduced to 3.9 μm, 320 nm, and 143 nm by increasing the PEG-PAA concentration from 50 to 75 and 100 $\mu g\,mL^{-1}$, respectively. It is obvious that the increasing amount of PEG-PAA is effective at reducing crystal size, presumably due to its adsorption on the crystal surface to compensate for the increased interfacial free energy.

The entrapping efficacy of the pDNA in the CaP/PEG-PAA hybrid particle was then determined by a centrifugation assay, in which the pDNA remaining in the supernatant after centrifugation at 15000 rpm for 3 min was quantified by agarose gel electrophoresis. Figure 2A shows a gel image and Figure 2B the result of the densitometry analysis. At polymer concentrations lower than 25 $\mu g\,mL^{-1}$, no bands were recognizable in the gel image for pDNA, essentially indicating that all of the pDNA in the system had been incorporated into the particles. The band intensity steeply increased beyond 100 $\mu g\,mL^{-1}$, becoming constant above 150 $\mu g\,mL^{-1}$. This indicates that, above concentrations of 150 $\mu g\,mL^{-1}$ of PEG-PAA,

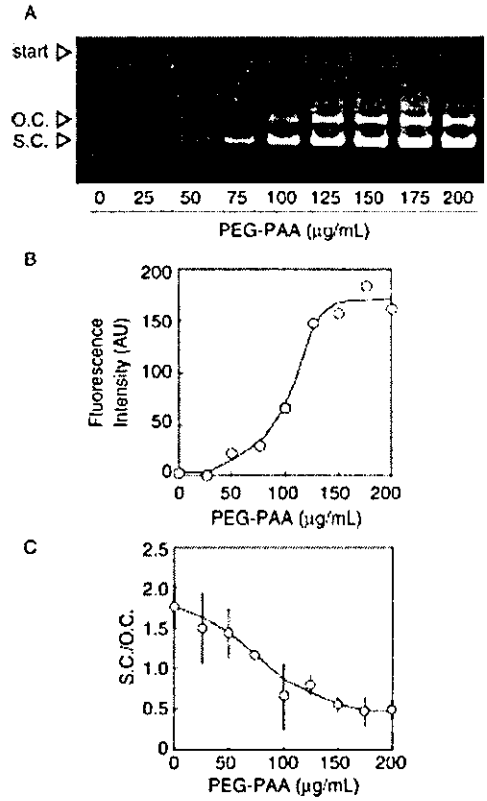

Figure 2. A,B) Centrifugation assay. A) Gel image (OC = open circular form, SC = supercoiled form of the plasmid DNA); B) densitometry analysis of the gel image. C) Enzyme protection assay. Error bars represent the standard deviation derived from triplicate experiments.

the pDNA was almost excluded from the particles. The decrease in the bound pDNA with increasing PEG-PAA concentration suggests that PEG-PAA and pDNA bind competitively to the calcium phosphate, and the exclusion of pDNA from the complex occurs at a higher polymer concentration, because the PAA segment itself may act as a nucleator or tying molecule during the formation of the complexes.[13,14]

Nuclease resistance of the pDNA associated with the CaP/PEG-PAA particles was then investigated using an endonuclease, deoxyribonuclease I (Dnase I). The metabolite of the pDNA was visualized by gel electrophoresis and the fluorescence intensity of the bands corresponding to the supercoiled (SC) and open circular (OC) forms was determined by densitometry analysis. The ratio of the fluorescence intensity of the SC, a native form, to the OC, a nicked form, was used as an index to quantitatively evaluate the degree of nuclease digestion as a function of the PEG-PAA concentration (Fig. 2C). Fluorescence intensity ratios for the naked pDNA before and after enzyme treatment were 3.26 ± 0.21 and 0.28 ± 0.12, respectively. Compared to the naked pDNA, degradation was significantly suppressed through association with CaP/PEG-PAA hybrid particles, particularly at lower polymer concentrations. In line with the trend in the inclusion efficacy of the pDNA into the hybrid particles seen in Figures 2A,B, the nuclease resistance substantially increased with decreasing polymer concentration.

Worth noting is the transfection activity of the hybrid particles to 293 cells evaluated at various concentrations of the PEG-PAA in the absence of fetal calf serum (FCS). As shown in Figure 3, the expression of the luciferase gene peaked at a polymer concentration of 50 $\mu g\,mL^{-1}$—six to seven times higher than with calcium phosphate alone (0 $\mu g\,mL^{-1}$). A similar trend in the activity–concentration profile was observed in the presence of FCS with a slightly lower expression than in the absence of FCS. Transfection experiments using HeLa cells showed a similar profile (data not shown), suggesting that the phenomenon is caused by the propensities of the vector itself. The improvement in the gene expression with an increase in the PEG-PAA concentration from 25 to 50 $\mu g\,mL^{-1}$ is significant, even though the entrapment efficacy and the enzyme tolerability of the pDNA in this concentration range are comparable (see Fig. 2). Presumably, the abrupt size reduction of the hybrid particles within this concentration range may play a substantial role in the steep increase in the transfection efficacy through the possible enhancement of their cellular internalization by endocytosis. Note that an enhancement of gene expression accompanied by the size reduction was reported for other synthetic vector systems composed of cationic polymers.[15,16] On the other hand, a gradual decrease in the expression level above 50 $\mu g\,mL^{-1}$ of the PEG-PAA may reasonably be due to the decreased entrapment efficacy of the pDNA in the hybrid particles.

In the calcium phosphate method, the control of the crystal size is the critical issue in obtaining a higher transfection efficacy. We demonstrated that the transfection efficacy of the CaP/pDNA system can be maximized via modulation of the particle size using a block copolymer. The advantage of the hybrid system is that the calcium phosphate core of the particles serves as a low-toxicity nanocontainer for the DNA, and the versatility of the chemical structure of the block copolymer may even allow the incorporation of functional molecules, such as the specific ligands for the cellular uptake on the distal end of the shell-forming segments.[17] It should be noted that the cytotoxicity of the hybrid particles in the PEG-PAA concentration range from 0 to 200 $\mu g\,mL^{-1}$ was indeed negligible (data not shown). With these desirable characteristics, calcium phosphate-based hybrid vectors might find wide in vivo applications as gene and other nucleic acid-based delivery systems with an appreciable biocompatibility.

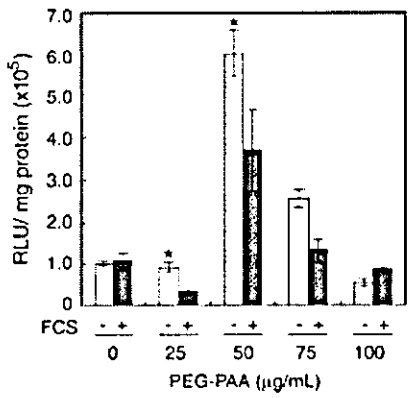

Figure 3. Effect of PEG-PAA concentration on the reporter gene expression. Samples were incubated with 293 cells in the absence (open bars) or presence (shaded bars) of 10% FCS. Results are expressed as RLU mg^{-1} of protein determined by BCA protein assay. Error bars represent standard error of the mean derived from triplicate transfection experiments. The symbol * indicates the statistical significance in the transfection levels ($p < 0.01$) between 25 and 50 $\mu g\,mL^{-1}$ of the PEG-PAA.

Experimental

Chemicals: Poly(ethylene glycol)-*block*-poly(aspartic acid) (PEG-PAA) was synthesized as previously described [12]. The molecular weight of the PEG segment was 12000 and the degree of polymerization of the PAA segment was 24. The plasmid pGL3 control luciferase reporter vector (Promega) was amplified with a competent *Escherichia coli* strain JM 109 and purified with a high-speed purification kit (Qiagen). The Dnase I solution was purchased from Takara Shuzo Co. All other reagents were used as received.

Preparation of Hybrid Vectors: pDNA dissolved in a 10 mM tris(hydroxymethyl)aminomethane-ethylene diamine-*N,N,N',N'*-tetraacetic acid solution (tris-EDTA) buffer (pH 7.4) was diluted with water and supplemented with a 2.5 M $CaCl_2$ solution to obtain a 2 × calcium/pDNA solution (pDNA 50 $\mu g\,mL^{-1}$, $CaCl_2$ 250 mM). The block copolymer, PEG-PAA, was dissolved in the phosphate solution (1.5 mM Na_2HPO_4, 50 mM *N*-2-hydroxyethylpiperazine-*N'*-2-ethanesulfonic acid (HEPES), 140 mM NaCl, pH 7.1) to obtain a 2 × phosphate/PEG-PAA solution (polymer concentration 0–400 $\mu g\,mL^{-1}$). One volume of the 2 × phosphate/PEG-PAA solution was added to an equal volume of the 2 × calcium/pDNA solution (final concentrations; pDNA 25 $\mu g\,mL^{-1}$, calcium ions 125 mM, phosphate ions 0.75 mM). After mixing with a vortex mixer for 3 s, the solutions were incubated at 25 °C for 24 h unless otherwise stated.

Turbidity Measurements: 2 × calcium/pDNA and 2 × phosphate/PEG-PAA solutions (1 mL) preincubated at 25 °C were directly mixed in a polystyrene cuvette. The transmittance at 350 nm was then measured for 90 s with continuous stirring at 1000 rpm at 25 °C.

Centrifugation Assays: Sample solutions (100 μL) prepared at polymer concentrations ranging from 0 to 200 μg mL^{-1} were incubated for 24 h at 25 °C and centrifuged at 15000 rpm for 3 min. The supernatant (20 μL) from each sample was recovered and applied to gel electrophoresis in order to determine the amount of the pDNA. Gel electrophoresis was conducted using a 0.9 % agarose gel and 40 mM tris-acetate buffer (10 mM EDTA). Images of the gels stained with ethidium bromide were acquired and analyzed using an ImageMaster-CL (Amersham Biosciences).

Enzyme Protection Assays: Dnase I solution (25 μL, 0.001 U μL^{-1}) was added to the complex solution (100 μL) and incubated for 1 h at 37 °C. An aliquot (25 μL) was withdrawn from the reaction mixture and 25 μL of a saturated EDTA solution was immediately added to stop the enzyme reaction. Samples were applied to gel electrophoresis and analyzed as described in the centrifugation assay.

Evaluation of Size of Complexes: The size of the particles formed at high polymer concentrations was determined by DLS as described in detail elsewhere [12]. The DLS measurements were carried out using a DLS-7000 instrument (Otsuka Electronics Co.). Vertically polarized light with a wavelength of 488 nm from an Ar-ion laser (15 mW) was used as the incident beam. All measurements were conducted at 25 °C, and data were analyzed by the cumulant method to determine the hydrodynamic diameters of the particles. Precipitates formed at low polymer concentrations were observed by light microscopy (Axiovert 200, Carl Zeiss Co.).

Transfection Experiments: 293 and HeLa cells were respectively grown in Dulbecco's modified Eagles medium (DMEM) supplemented with 10 % FCS at 37 °C in a 5 % CO_2 humidified atmosphere. After 24 h of incubation in six-well culture plates, the cells were rinsed with serum-free DMEM and 1000 μL of culture medium with or without FCS was added to each well. Immediately before the transfection, the particle solutions were suspended by pipetting and 100 μL was added to each well. After 6 h of incubation, the medium was replaced with fresh medium containing 10 % FCS. Cells were incubated for an additional 24 h in the complete medium. A luciferase assay was conducted with a luminometer (Fluoroskan Ascent FL, Labsystems) using a Promega kit according to the manufacturer's protocol. Results were expressed as relative light units (RLU) per milligram of protein determined using a BCA protein assay kit (Pierce; BCA = bicinchoninic acid). The error bars represent standard error of mean derived from the triplicate transfection experiments.

Cytotoxicity Assays: 293 and HeLa cells were used for the cytotoxicity assay. Cells were plated in 96-well plates at a density of 10000 cells per well and allowed to adhere overnight. The hybrid particles, formed at the varying polymer concentrations from 0 to 200 μg mL^{-1} were added as suspension in the medium to the semiconfluent cellular monolayer in the presence of 10 % FCS, and incubated for 24 h at 37 °C. Subsequently, the cell viability was determined by a 3-(4,5-dimethylthiazol-2-yl)-2,5-diphenyltetrazolium bromide (MTT) assay.

Received: August 2, 2003
Final version: January 5, 2004

[1] *Self-Assembling Complexes for Gene Delivery* (Eds: A. V. Kabanov, P. L. Felgner, L. W. Seymour), John Wiley, Chichester, UK **1998**.
[2] D. Luo, W. M. Saltzman, *Nat. Biotechnol.* **2000**, *18*, 33.
[3] A. Akinc, D. M. Lynn, D. G. Anderson, R. Langer, *J. Am. Chem. Soc.* **2003**, *125*, 5316.
[4] O. Boussif, F. Lezoualch, M. A. Zanta, M. D. Mergny, D. Ssherman, B. Demeneix, J. P. Behr, *Proc. Natl. Acad. Sci. USA* **1995**, *52*, 7297.
[5] M. Cotten, F. Langlerouault, H. Kirlappos, E. Wagner, K. Mechtler, M. Zenke, H. Beug, M. L. Birnstiel, *Proc. Natl. Acad. Sci. USA* **1990**, *87*, 4033.
[6] Y. Kakzizawa, K. Kataoka, *Adv. Drug Delivery Rev.* **2002**, *54*, 223.
[7] S. Katayose, K. Kataoka, *Bioconjugate Chem.* **1997**, *8*, 702.
[8] F. L. Graham, A. J. van der Eb, *Virology* **1997**, *52*, 456.
[9] C. Chen, H. Okayama, *Mol. Cell. Biol.* **1987**, *7*, 2745.
[10] H. Tolou, *Anal. Biochem.* **1993**, *215*, 156.
[11] M. Jordan, A. Schallhorn, F. M. Wurm, *Nucleic Acids Res.* **1996**, *624*, 596.
[12] Y. Kakizawa, K. Kataoka, *Langmuir* **2002**, *12*, 4539.
[13] J. V. Gracia-Ramas, P. Carmona, A. Hidalgo, *J. Colloid Interface Sci.* **1981**, *83*, 479.
[14] S. I. Stupp, G. W. Ciegler, *J. Biomed. Mater. Res.* **1992**, *26*, 169.
[15] C. L. Gebhart, S. Sriadibhatla, S. Vinogradov, P. Lemieux, V. Alakhov, A. V. Kabanov, *Bioconjugate Chem.* **2002**, *13*, 937.
[16] E. Wagner, M. Cotten, R. Foisner, M. L. Birnstiel, *Proc. Natl. Acad. Sci. USA* **1991**, *88*, 4255.
[17] K. Kataoka, A. Harada, D. Wakebayashi, Y. Nagasaki, *Macromolecules* **1999**, *32*, 6892.

Growth of Silicon Oxide in Thin Film Block Copolymer Scaffolds**

By *Dong Ha Kim*, *Xinqiao Jia*, *Zhiqun Lin*, *Kathryn W. Guarini*, and *Thomas P. Russell**

Numerous fabrication methods have been reported to generate surfaces patterned with regularly sized and spaced features on the nanometer-scale. Due to their ability to self-assemble into a variety of ordered nanoscale morphologies, block copolymers offer an attractive route to overcome the limitations of conventional lithographic techniques.[1–11] Silicon dioxide has tremendous promise for applications ranging from microelectronic to photonic devices, and significant efforts have been made to fabricate tailored structures.[12–16] Combining the self-assembly of blocks with the synthesis of silicon oxide may offer a unique approach to device fabrication.

[*] Prof. T. P. Russell, Dr. D. H. Kim,[+] Dr. X. Jia,[++] Dr. Z. Lin[+++]
Silvio O. Conte National Center for Polymer Research
Polymer Science and Engineering Department
University of Massachusetts at Amherst
Amherst, MA 01003 (USA)
E-mail: russell@mail.pse.umass.edu
K. W. Guarini
IBM T. J. Watson Research Center
Yorktown Heights, NY 10598 (USA)
[+] Current address: Max Planck Institute for Polymer Research, Ackermannweg 10, D55128 Mainz, Germany.
[++] Current address: Department of Chemical Engineering, Massachusetts Institute of Technology, Cambridge, MA 02139, USA.
[+++] Current address: Department of Materials Science and Engineering, University of Illinois at Urbana-Champaign, Urbana, IL 61801, USA.
[**] We are grateful for the financial support of the Department of Energy, Basic Energy Sciences under contract DE-FG02-96ER45612, National Science Foundation under the partnership in Nanotechnology (CTR-9871782), and NSF-sponsored Material Research Science and Engineering Center at the University of Massachusetts at Amherst.

  DOI: 10.1002/adma.200404906